University of Stavanger

Faculty of Science and Technology

# MASTER'S THESIS

| | |
|---|---|
| Study program/ Specialization:<br><br>Industrial Economy / Drilling & Project Management | Spring semester, 2012<br><br>Open / ~~Restricted access~~ |
| Writer:<br>Cecilie H.S. Eide | ……<br>(Writer's signature) |
| Faculty supervisor: Dr. E. Kaarstad<br><br>External supervisor(s): N/A | |
| Title of thesis:<br><br>Understanding Drilling Induced Fractures | |
| Credits (ECTS): 30 | |
| Key words:<br><br>In-situ stresses, Tensile failure, Borehole image log, ECD, Drilling induced fractures, Temperature effect | Pages: …77…<br><br>+ enclosure: ……<br><br>Stavanger, 14 June 2012 |

## Abstract

Oil and gas production is moving to harsher geological conditions such as deep water drilling and high-pressure high-temperature reservoirs, so accurate knowledge of wellbore stability is crucial. The main causes of wellbore instability are high pore pressure in the formation, drilling induced disturbance of stable formations and the possible chemical reactions between the reservoir formation and the drilling and completion fluids. The thesis has studied the occurrence of drilling induced fractures, which can eventually cause fluid losses to the formation, hence become a costly issue during drilling. Borehole image tool are the only tool as of today that can detect drilling induced fractures, however one would like to prevent them from occurring. The thesis is interested in examine what can be the primary effect of their occurrence, and have chosen to focus on the effect of temperature. A new fracturing model was also introduced in this examination, where three scenarios were developed. These scenarios provided important information on the fracture gradient's sensitivity towards temperature. Finally, the coefficient of thermal expansion was suggested to investigate further as it may have a bigger impact on the fracture gradient than initially presumed. Additionally, the importance of time-dependent downhole MWD data along with effective ECD management was accentuated.

# 1. Table of Contents

## Acknowledgement

I would like to express my appreciation to dr. Eirik Kårstad at the University of Stavanger, who provided me an interesting Master Thesis. I appreciate our discussions, his engagement, support, and knowledge as he is as a skilled and experienced supervisor.

I also want to thank Statoil, which provided data for this study. Finally, I give my thanks to Mesfin Agonafir Belayneh for helpful discussion and provided literature.

## List of Figures

## List of Tables

## Nomenclature

| | |
|---|---|
| A | Area |
| a | Borehole radius |
| d | Mud weight |
| *d* | Formation depth |
| $\alpha$ | Coefficient of linear thermal expansion |
| $\phi$ | Angle of internal Friction |
| $\beta$ | Angle, rock specimen, Biot's poroelastic constant |
| $\sigma$ | Normal stress |
| $\tau$ | Shear stress |
| $\tau_0$ | Cohesive strength |
| E | Young's modulus |
| $\upsilon$ | Poisson's ratio |
| F | Force |
| $f_e$ | Effective stress coefficient |
| $\varepsilon$ | Strain |
| $G_f$ | Formation fracture gradient (Eaton formula) |
| $\Delta l$ | Deformation change in length |
| l | Length |
| $J_2$ | Second deviatoric invariant |
| $K_{S1}$ | Scaling effect of Poisson's ratio |
| $K_{S2}$ | Scaling effect of temperature |
| $\Delta T$ | Temperature change |
| $\sigma_h$ | Minimum horizontal stress |
| $\sigma_H$ | Maximum horizontal stress |
| $\sigma_v$ | Vertical stress |
| $\sigma_r$ | Radial stress |
| $\sigma_t$ | Tangential stress |
| $\sigma_a$ | Axial stress |
| $\sigma_m$ | Average stress |
| $\sigma_T$ | Stress due to temperature change |
| $\sigma_{z1}$ | Plain strain |
| $\sigma_{z2}$ | Plain stress |
| P | Pressure |
| $P_o=P_p$ | Pore pressure |
| $P_T$ | Fracture pressure including temperature change |
| $P_w$ | Fracture pressure, wellbore pressure |
| $P_{wf}$ | Wellbore fracture pressure |
| $R_W$ | Well radius |
| t | Filter-cake thickness |
| T | Temperature |
| $T_0$ | Initial temperature = VFT |
| $z^0$ | Virgin formation stress |
| Y | Yield strength |

## Abbreviations

| | |
|---|---|
| BHT | Bottom Hole Temperature |
| ECD | Equivalent Circulating Density |
| EMW | Equivalent Mud Weight |
| ESD | Equivalent Static Density |
| DED | Distortional Energy Density |
| DIF | Drilling Induced Fracture |
| FG | Fracture Gradient |
| FIT | Formation Integrity Test |
| FMI | Formation Micro Imager |
| LOT | Leak Off Test |
| LWD | Logging While Drilling |
| MD | Measured Depth |
| MDT | Modular Formation Dynamics Tester |
| MWD | Measurement While Drilling |
| OBG | Overburden Gradient |
| PP | Pore Pressure |
| PVT | Pressure, Volume, Temperature |
| ShG = Sh | Minimum Horizontal Pressure, $\sigma_h$ |
| SH | Maximum Horizontal Pressure, $\sigma_H$ |
| TD | True Depth |
| TVD | True Vertical Depth |
| VFT | Virgin Formation Temperature |

## 2. Introduction

One of the most costly issues in the drilling industry is loss of fluids to the formation. Fluid loss is a result of tensile failure, thereby fraction of the formation. As drilling moves into harsher environments and deeper wells, it becomes even more crucial to avoid drilling induced fractures as the mud-window decreases. To date, borehole-imaging tools are being used to identify natural fractures, analyze geological structures, and to reconstruct the geometry of reservoir units. However, these instruments can also be used to interpret rock stresses and to assess rock mechanical properties. One challenge to interpret rock stresses from image log is the limited information on how to couple the image to the environment (e.g. pressure and temperature) when drilling induced fractures were created. The thesis will analyze a well where drilling induced fractures are documented in order to improve the understanding of their occurrence. The study's purpose is to evaluate if temperature is the first order effect that influences the initiation of these fractures, as well as studying a new fracturing model that includes this effect. This theoretical model is the latest model proposed in research to determine an accurate fracture gradient, as it is believed to account for important mechanisms that contribute to formation fracturing.

In the essence of borehole failure analysis, two failure modes can occur, that is compressive failure and tensile failure. Since the purpose of the thesis is to study drilling induced fractures, the thesis will have its primary focus on the tensile failure mode. It is important to keep in mind that compressive failure is also presence, so one does not only think of "one side of the story". Hence, differences between the two failure modes will be addressed where it is relevant. Furthermore, the thesis has chosen to focus on the temperature effect and those parameters that are included in the new fracturing model relating drilling induced fracturing.

The thesis will first outline the basic theory of rock mechanics in order to understand the mechanisms behind failure theory and how stress interacts in the formation and around the borehole. Failure criteria and the effective circulating densities are then outlined, followed by a description of the fracture process, fracture determination on the borehole wall, and different methods in determine the fracture gradient.

The new fracturing model is then systematically outlined followed by a presentation of the borehole-imaging tool. This chapter will also present pictures of the different types of fractures. Thermal effect is then thoroughly described, followed by a review of other studies regarding this subject and their conclusions. Finally, the thesis gives a detailed analyse of a well in the North Sea which has proved drilling induced fractures from a borehole image log. The thesis has then analysed above-mentioned parameters that may have caused these fractures and proposed improvements of the model and a suggestions of further work.

The thesis' restrictions are given by the limited data. A big challenge was to retrieve time-dependent downhole data, which was necessary in order to conduct a fully consistent analysis. Additionally, a significant report was retrieved late in the study. There was neither access of any modelling programs in order to simulate data. AGPS Harvard reference style is used.

# 3. Theory

Just as a tennis racket needs to handle a dynamic impact load from a high-speed tennis ball, it also needs to handle a possible impact of hard ground. Drilling equipment needs to penetrate different rock materials in a suitable and sufficient way and at the same time not impose the rock extensive load that can change the formation's integrity and affect the stability of the well. The importance of understanding the fundamentals of solid mechanics is crucial in order to explain drilling induced fracturing.

## 3.1. Rock Mechanics

The two key elements of solid mechanics are stress and strain. The definition of stress is the average force acting over an area (Fjaer et al. 2008).

$$\sigma = \frac{F}{A}$$

**Eq. 1 Definition of stress**

The area may be a surface, or an imaginary plane inside a material, where it is independent of the size and shape of the body. It is, however, dependent on its orientation. There are two types of stresses resulting from the equilibrium condition. These are normal stress, $\sigma$, which act normal to the plane, and shear stress, $\tau$, which acts along the plane. Normal stress may result in tensile or compressive failure, while shear stress result in shear failure (material is sheared or slipped along a plane). In all, there are nine different components that is required in order to determine the state of stress at one point:

$$[\sigma] = \begin{bmatrix} \sigma_x & \tau_{xy} & \tau_{xz} \\ \tau_{xy} & \sigma_y & \tau_{yz} \\ \tau_{xz} & \tau_{yz} & \sigma_z \end{bmatrix}$$

**Eq. 2 Stress matrix**

In contrast to stress, strain can be measured. The relationship between stress and strain, also known as Hooke's law, is therefore an important equation.

$$\sigma = E \cdot \varepsilon$$

**Eq. 3 Hooke's law**

E is defined as the constitutive relation {Young's modulus}, and is a measurement of the material's stiffness, i.e. its resistance of being compressed. Strain is when the body undergoes a deformation or displacement due to external forces, so any point within the body will be given a new position. It is defined as the deformation divided by the original dimension, and is categorized as either *engineering* strain, where it uses the original dimension in the analysis, and *scientific* strain, where the actual dimension, which will change in time, is used.

$$\varepsilon = \frac{\Delta l}{l}$$

**Eq. 4 Definition of strain**

This equation will not be valid if it involves large deformations.

### 3.2. Principal stresses

Principal stresses are important in any failure analysis of materials as it represent the maximum and the minimum stresses in the rock. The stress state is normally divided into two components, which are *average hydrostatic stress*, and *deviatoric stress*. It is under the deviatoric load (shape change) that the material will fail, hence why this component is an important part of the failure criteria's used in rock mechanics. The general interpretation of principal stresses can act in three states; hydrostatic stress, two principal stress state, and in a triaxial stress state.

Hydrostatic stress is when all principal stresses are equal, which means that principal stresses exist in all directions. Subsequently, no shear stresses will exist. This is also shown in the figure below.

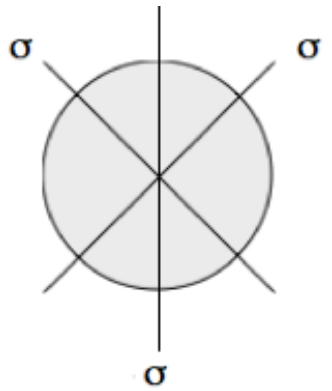


$$[\sigma] = \begin{bmatrix} \sigma & 0 & 0 \\ 0 & \sigma & 0 \\ 0 & 0 & \sigma \end{bmatrix}$$

**Figure 1 Hydrostatic state of stress (redrawn from Aadnoy & Looyeh, 2010, p 30)**

The second stress state is when two principal stresses are equal. This stress state is applied in the laboratory testing of core plugs for e.g. testing wellbore instability analyses. The following geometry is then present:

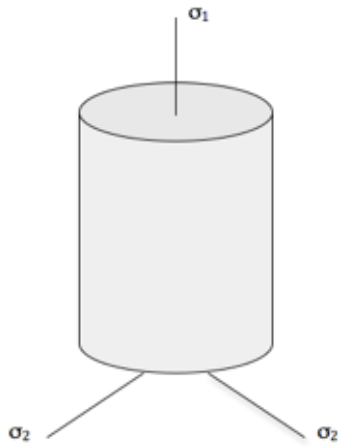


$$[\sigma] = \begin{bmatrix} \sigma_1 & 0 & 0 \\ 0 & \sigma_2 & 0 \\ 0 & 0 & \sigma_2 \end{bmatrix}$$

**Figure 2 Two equal principal stresses (redrawn from Aadnoy & Looyeh, 2010, p 31)**

The third stress state is called a triaxial stress state. None of the stresses are then equal. This is also shown in Figure 3 where the principal stresses can be defined as:

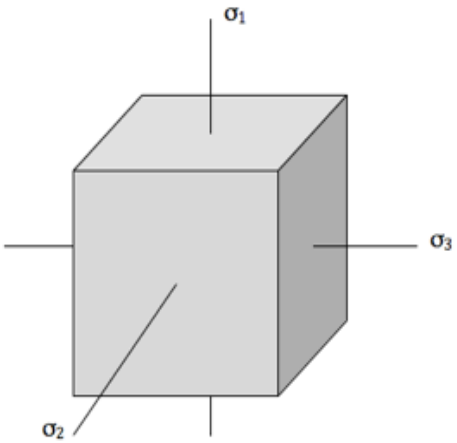


$$[\sigma] = \begin{bmatrix} \sigma_x & \tau_{xy} & \tau_{xz} \\ \tau_{xy} & \sigma_y & \tau_{yz} \\ \tau_{xz} & \tau_{xz} & \sigma_z \end{bmatrix} = \begin{bmatrix} \sigma_1 & 0 & 0 \\ 0 & \sigma_2 & 0 \\ 0 & 0 & \sigma_3 \end{bmatrix}$$

**Figure 3 Triaxial stress state (redrawn from Aadnoy & Looyeh, 2010, p 31)**

The principal stresses $\sigma_1$, $\sigma_2$, $\sigma_3$ are also called the *eigenvalues* of the stress state matrix, and will always be in the following order $\sigma_1 > \sigma_2 > \sigma_3$. The *eigenvalues* are calculated by the following equations that are later used in failure analyses, i.e. in Mohr-Coulomb failure criterion (Aadnoy & Chenevert, 1987).

$$\sigma_1 = \sigma_r = P_w$$

$$\sigma_{2,3} = \frac{1}{2}\left(\sigma_\theta + \sigma_z\right) \pm \frac{1}{2}\left[\left(\sigma_\theta - \sigma_z\right)^2 + 4\left(\tau_{\theta z}\right)^2\right]^{\frac{1}{2}}$$

**Eq. 5 Principal stresses**

The subscripts are then rearranged in the ascending order, as previously described. The components $\sigma_r$, $\sigma_z$, and $\sigma\theta$ represents the radial, axial and tangential stress respectively. The thesis will address rock failure analysis in detail in chapter 4.

### 3.3. In-situ stresses

Rocks are subjected to various stresses at any point in the formation. The conditions of the in-situ stresses, also called far-field stresses, are in an equilibrium state of an undisturbed ground. One of the main reasons for determining in-situ stresses is to find basic data on the formations stress state. As suggested by Aadnoy and Bell (1998), the ability to determine these data directly from a borehole contributes to a substantial decrease in drilling cost due to a thoroughly planning of the drilling and production processes.

The in-situ stresses follow the same configuration as the principal stresses. The weight of the overlaying formation and fluid is referred to as the vertical stress or overburden stress, $\sigma_v$. Moreover, $\sigma_v$ may tilt due to tectonic stresses. Salt domes or magma intruding in the nearby formation may affect this vertical stress state. The overburden stress normally tends to expand the underlying rocks in the lateral direction, which is also known as the effect of Poisson's ratio (Fjaer et al. 2008). The nearby materials then again restrict this lateral movement, and therefore causes horizontal lateral stresses $\sigma_H$ (maximum horizontal stress), and $\sigma_h$ (minimum horizontal stress) to form. Examples that may cause change in the horizontal stresses could be earthquakes, and/or increase or reduction in formation temperature.

The following figure shows the relation between in-situ stresses and principal stresses:

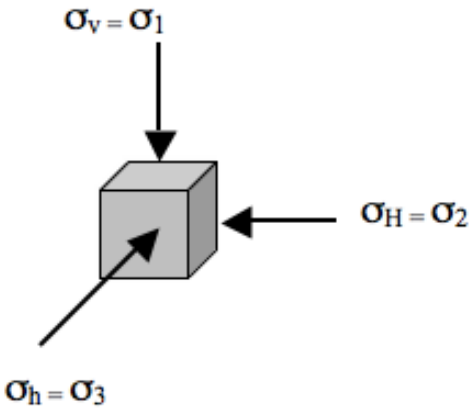


**Figure 4 In-situ principal stresses for a drilled vertical well (redrawn from Aadnoy & Looyeh, 2011 p.108)**

The order of the *eigenvalues* also apply for the in-situ principals $\sigma_v > \sigma_H > \sigma_h$, where all of the three principal stresses have different magnitudes.

### 3.4. Estimation and measurements of in-situ stresses

Management of ECD, prediction and evaluation of the different pressure curves, and drilling safety are all examples that is influenced by the accuracy of estimated and measured in-situ stresses. Determination of formation pore pressure and in-situ stresses are also of great importance as they all grant a guideline in the selection of casing design, and critical pressures.

Overburden stress is normally obtained from density logs, and the horizontal stresses are obtained by solving the fracture pressure equation and the stress transformation equations, simultaneously. The horizontal stresses were traditionally estimated to be equal, due to lack of data acquisition. They depend greatly on the Poisson's ratio since the in-situ stresses are related to one another. This is explained by the overburden stress that squeezes the rock vertically, hence pushing the rock horizontally. For example, a rock with a high Poisson's ratio will have a higher horizontal stress, than a rock with lower Poisson's ratio (Aadnoy &Looyeh, 2011). In order to calculate the horizontal stress, considering equal magnitude, i.e. $\sigma_h = \sigma_H$, and only due to overburden stress, the following empirical equation is proposed (Avasthi, Goodman, and Jansson, 2000):

$$\sigma_h = \frac{\upsilon}{1-\upsilon}\left(\sigma_v - \beta P_o\right) + \beta P_o$$

**Eq. 6 Empirical horizontal stress equation**

Where β is Biot's poroelastic constant. This formula is normally used when there are no requirements of introducing other horizontal stress terms.

In the determination of the fracture gradient, there are a direct approach and an indirect approach in measuring the in-situ stresses (Avasthi, Goodman and Jansson, 2000). A hydraulic fracturing test (direct approach) is the most effective method in measuring the magnitude of the minimum horizontal in-situ stress in the wellbore. However, only a small set of data can be obtained, so the stress tensor is often calibrated to the leak-off test (LOT) pressure or the mini-fracture test data, shifting the log based stress profile linearly.

The table below summarizes the methods that are typically used in the measurement and/or estimation of the in-situ stresses as well as the formation pore pressure.

**Table 1 Methods in estimating and measuring in-situ stresses (Aadnoy and Looyeh, 2011, p. 112)**

| Measurement Element | Type of stress | Measurement Techniques | Estimation Techniques |
|---|---|---|---|
| Stress Magnitude | $\sigma_v$ | Density Log | |
| | $\sigma_H$ | | Breakout<br>Mud Weight<br>Observation of Wellbore Failure |
| | $\sigma_h$ | Hydraulic Fracturing | LOT<br>Formation Integrity Test<br>Lost Circulation<br>Drilling induced fractures |
| Stress Orientation | $\sigma_H$ or $\sigma_h$ | Cross Dipole<br>Mini-frac<br>Hydraulic Fracture Test<br>Drilling induced fractures<br>Breakouts | Fault Direction<br>Natural Fault Direction |
| Formation Pore Pressure | $P_o$ | Drillstem Test<br>Repeat Formation Test<br>Modular Formation Dynamics Test<br>LWD<br>Measured Direct Test | Density Log<br>Sonic Log<br>Seismic Velocity<br>Mud Weight Used |

As seen from the table, LOT is also used technique to estimate wellbore's fracture pressure capacity. This test will be elaborated in detail later in the thesis. A formation integrity test (FIT-test) is an alternative to a LOT. As the LOT will overestimate the fracture pressure (since the test stops as the fractures has already been initiated), the FIT-test assures that the fracture initiation pressure is larger than the FIT pressure (Sh > FIT). A FIT will not estimate minimum horizontal stress, but assures that the formation will not fracture as long as the mud pressure is lower than the FIT test pressure.

A mini fracture test (mini-frac) estimates the same magnitude and orientation as a LOT, but is often performed before the main hydraulic fracturing treatment in order to obtain critical job design and execution data. The result from the test often aids in the optimization of final drilling parameters and treatment parameters. The orientation of the in-situ stress field can also be derived from studying the fracture angle on the image log. That is done by the *inversion technique*.

#### 3.4.1. **The inversion technique**

The inversion technique is a useful tool in simulating the in-situ stress field's direction and magnitude in order to e.g. predict fracture gradient for future wells. A typical fracture pattern that appears on the image log when the stress field is not aligned in the wellbore direction is a zigzag pattern, or *en echelon* pattern. The fracture angle, $\beta$, contains significant information of the in-situ stress field's orientation. Moreover, the technique uses an advanced data program that contains vital input parameters, for several depths and runs in order to simulate the in-situ stress field orientation. These parameters are e.g. formation pore pressure, overburden stress at each fracture location, and directional data (borehole inclination and azimuth).

### 3.5. Stresses around borehole

The stress around the borehole wall is determined by the in-situ stresses and the formation's respond to load. Prior to drilling, the formation is normally in a balanced stress state, and the principal stresses are then known as in-situ stresses. Once drilling has commenced, the stress state will change due to the new geometrical situation. Disturbance of the formation's pore pressure, reduction of cohesive strength and change in capillary forces (the ability of liquid to flow in tight spaces on a molecular level) are then some of the results that occur due to drilling and introducing fluid into the formation.

Far field stresses and wellbore stresses are important in the analysis of wellbore rock mechanics. As described above, the wellbore stresses will act on the formation at the mud-formation interface. On the contrary, the borehole will not influence the far-field

stresses, as they exist far away from the wellbore. The figure and table below illustrates the relation of the Cartesian coordinates (far-field stresses) and the cylindrical coordinates (wellbore stresses) in a vertical wellbore.

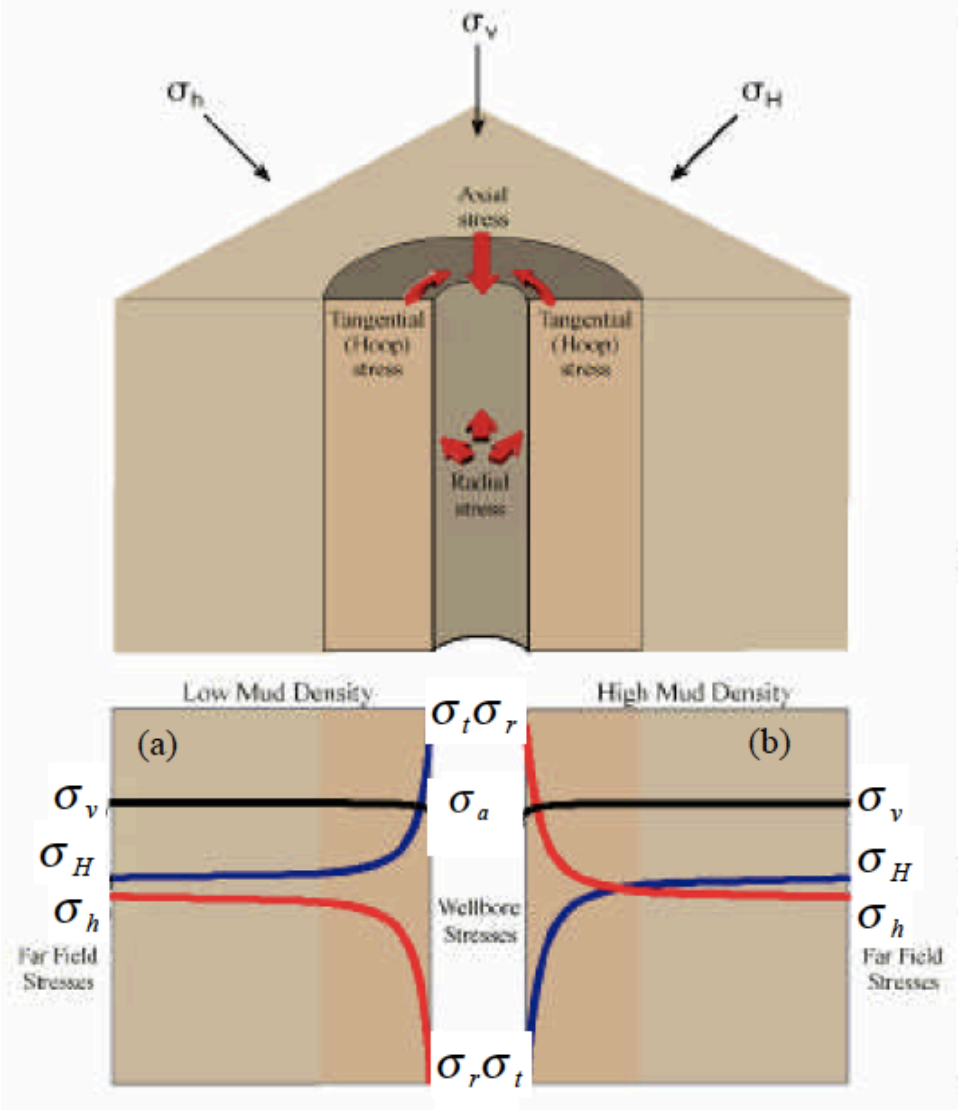


**Figure 5 Relation between far-field stresses and wellbore stresses (Rezmer-Cooper, Bratton & Krabbe, 2000)**

The following table display the transformations of stresses observed in the vertical well:

**Table 2 Wellbore stresses and far-field stress transformation in a vertical well.**

| Wellbore stresses | Far-field stresses |
|---|---|
| Axial stress ($\sigma_a$) - acts along the axis of the wellbore | Vertical stress ($\sigma_v$) |
| Tangential stress ($\sigma_t$) - acts along the circumference of the borehole | Maximum horizontal stress ($\sigma_H$) |
| Radial stress ($\sigma_r$) – acts on the borehole wall | Minimum horizontal stress ($\sigma_h$) |

The radial stress is highly controllable by the driller (e.g. pressure of drilling mud), whereas the two remaining stresses are less influential as they are controlled by the far-field stresses.

### 3.6. The Kirsch's equations

Kirsch was the first to present the stress distribution around a circular hole in a plate with stress on one side. The Kirsch's equations are based on linear elasticity and assume homogeneous and isotropic rock properties (Fjaer et al. 2008). The figure below present the stress nomenclature that are used in his equations:

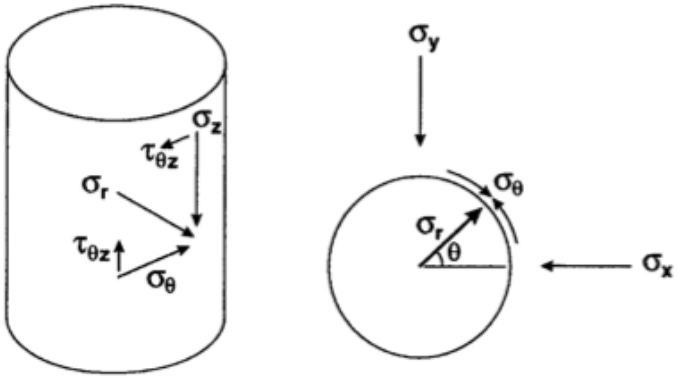


**Figure 6 Stresses on a borehole wall (Aadnoy & Bell, 1998)**

Where $\sigma_r$ is the radial stress, $\sigma_\theta$ is tangential stress, $\sigma_z$ is axial stress. Kirsch's general elastic solution, assuming plane strain normal to the borehole axis, and non-porous material or porous material with constant pore pressure, is then

$$\sigma_r = \frac{\sigma_x + \sigma_y}{2}\left(1 - \frac{R_W^2}{r^2}\right) + \frac{\sigma_x - \sigma_y}{2}\left(1 + 3\frac{R_W^4}{r^4} - 4\frac{R_W^2}{r^2}\right)\cos 2\theta + \tau_{xy}\left(1 + 3\frac{R_W^4}{r^4} - 4\frac{R_W^2}{r^2}\right)\sin 2\theta + p_W \frac{R_W^2}{r^2}$$

$$\sigma_\theta = \frac{\sigma_x + \sigma_y}{2}\left(1 + \frac{R_W^2}{r^2}\right) - \frac{\sigma_x - \sigma_y}{2}\left(1 + 3\frac{R_W^4}{r^4}\right)\cos 2\theta - \tau_{xy}\left(1 + 3\frac{R_W^4}{r^4}\right)\sin 2\theta - p_W \frac{R_W^2}{r^2}$$

$$\sigma_z = \sigma_z^0 - \upsilon\left[2\left(\sigma_x - \sigma_y\right)\frac{R_W^2}{r^2}\cos 2\theta + 4\tau_{xy}\frac{R_W^2}{r^2}\sin 2\theta\right]$$

$$\tau_{r\theta} = \frac{\sigma_y - \sigma_x}{2}\left(1 - 3\frac{R_W^4}{r^4} + 2\frac{R_W^2}{r^2}\right)\sin 2\theta + \tau_{xy}\left(1 - 3\frac{R_W^4}{r^4} + 2\frac{R_W^2}{r^2}\right)\cos 2\theta$$

$$\tau_{\theta z} = \left(-\tau_{xz}\sin\theta + \tau_{yz}\cos\theta\right)\left(1 + \frac{R_W^2}{r^2}\right)$$

$$\tau_{rz} = \left(\tau_{xz}\cos\theta + \tau_{yz}\sin\theta\right)\left(1 - \frac{R_W^2}{r^2}\right)$$

**Eq. 7 General Elastic Solution**

Where the subscript *o* on the stress denote z, refers to the virgin formation stress, and υ is the Poisson's ratio. $R_W$ is the well radius, and $r^2$ / $r^4$ is given by the borehole influences, though these will vanish as r increases. The stresses will vary with position around the wellbore, thus, depending on the angle θ. The shear stresses are normally non-zero, hence Kirsch's equations reduces to:

$$\sigma_r = P_w$$

$$\sigma_\theta = \sigma_x + \sigma_y - P_w - 2\left(\sigma_x - \sigma_y\right)\cos 2\theta - 4\tau_{xy}\sin 2\theta$$

$$\sigma_{z1=} = \sigma_{zz} - 2\upsilon\left(\sigma_x - \sigma_y\right)\cos 2\theta - 4\upsilon\tau_{xy}\sin 2\theta$$

$$\sigma_{z2} = \sigma_{zz}$$

$$\tau_{r\theta} = \tau_{rz} = 0$$

$$\tau_{\theta z} = 2\left(-\tau_{xy}\sin\theta + \tau_{yz}\cos\theta\right)$$

**Eq. 8 Kirsch Equations**

$\sigma_{z1}$ → plain strain
$\sigma_{z2}$ → plain stress

As seen from Kirsch's equation, fracture occurs when the minimum in-situ stress exceeds. In drilling operations, these equations uses a non-penetrating boundary condition and becomes (Aadnoy, Kaarstad and Belayneh, 2007):

$$P_{wf} = 2\sigma_h - P_p$$

**Eq. 9 Simplified Kirsch equation in drilling operation**

A non-penetrating boundary condition is when fluids build up a filter cake barrier during the drilling operation, assuming a perfect mudcake so there will be no filtration loss. A penetrating boundary condition will then be fluid pumped into the formation (Aadnoy et al. 2008). In spite of Kirsch's' "popularity", the equations strongly underestimate fracture pressure, thus new models have been developed in order to provide a more accurate and reliable fracturing model. One of these models will be presented later. First, the process of borehole failure will be presented.

## 4. Borehole Failure

Borehole failure are dependent on interrelated factors such as orientation, formation pore pressure, rock compressive strength, wellbore azimuth, and the in-situ stress magnitude where two orthogonal stresses (axial and tangential stress) cause shear failure, and a single tensile stress causing a tensile failure (Aadnoy et al. 2009).

There are in all, nine modes of failure: six modes of shear failure and three modes of tensile failure. Shear, or compression failure is when the pressure inside the borehole is lower than the pore pressure (underbalanced condition) and may eventually cause collapse or breakouts of parts of the borehole wall. Tensile failure is when the wellbore pressure exceeds the formation's fracture pressure (overbalanced drilling condition), and may lead to fracturing the borehole wall (Aadnoy & Looyeh, 2011). Consequently, an optimum mud weight will therefore be a crucial parameter in a sound drilling operation. The different failures modes may happen independently, sequentially or simultaneously, and are presented by the following figure:

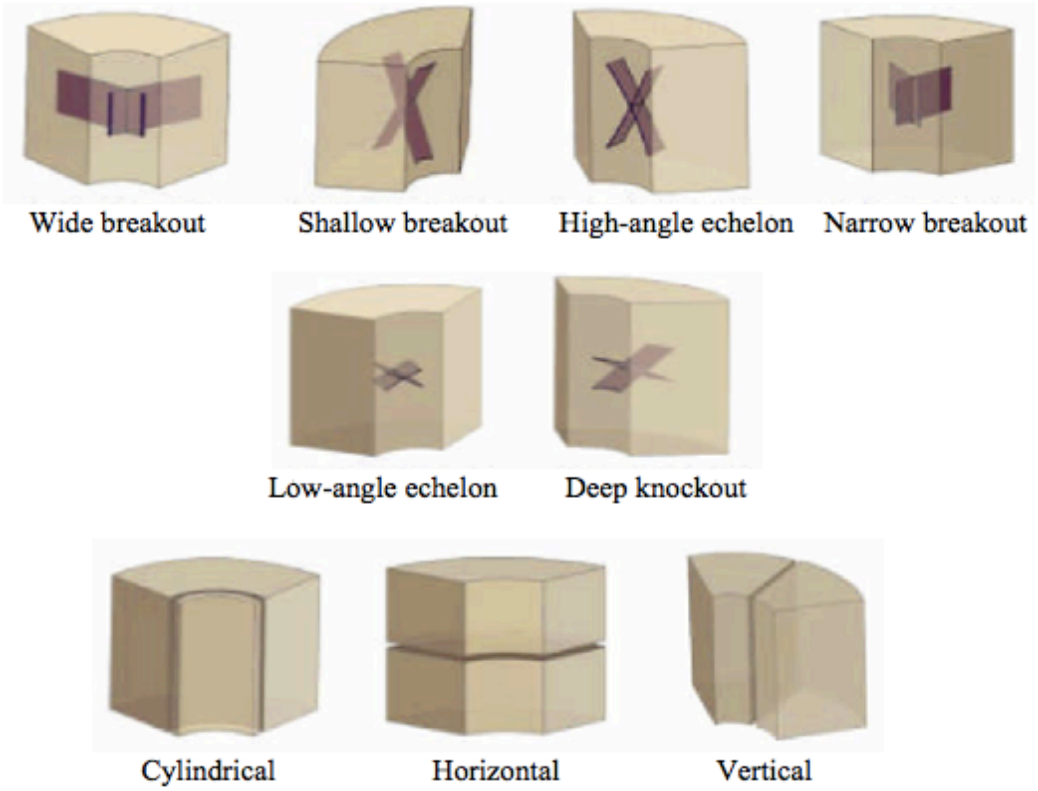


**Figure 7 Failure Modes (Rezmer-Cooper, Bratton & Krabbe, 2000)**

The first the six figures illustrate the different modes of shear failure, while the remaining bottom-three represents tensile failure modes.

### 4.1. Brittle and ductile behavior

A rock's property of brittleness or ductility has an important contribution on the rock's restiveness towards failure, and the rock exhibits either of these two types of behaviour depending on mineralogy, microstructure, and temperature (Jaeger, Cook and Zimmerman, 2007, p.84) A brittle rock will fail as strain increases, hence it undergoes very little plastic deformation. A ductile rock, on the other hand, has the ability to support an increasing load as it deforms, hence it behaves more plastic (permanent change of shape without fracturing). A rock's ductile/brittle behaviour can, however, be affected by pressure and temperature (Jaeger, Cook and Zimmerman, 2007). For example, both higher pressure and higher temperature encourages ductility. Consequently, the brittle/ductile *transition temperature* will also increase, as the confining stress increases.

The two sets of rock behaviour is described by the relationship between stress and strain in the following figure:

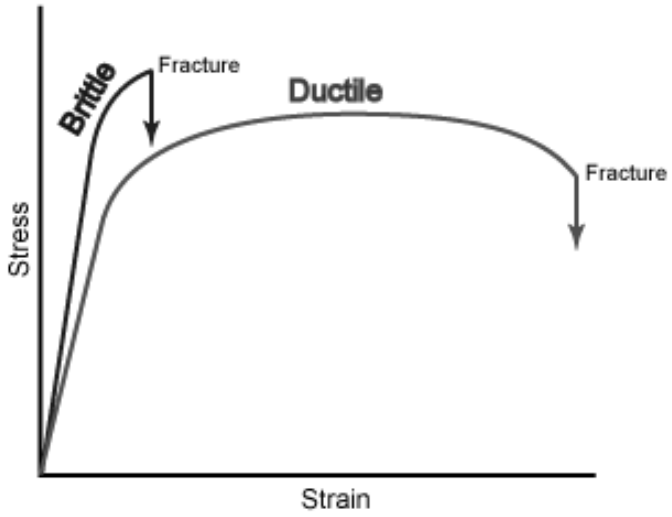


**Figure 8 Rock behaviour**

When the ductile graph transform from its linear behaviour (as seen in the figure above), is when the rock starts *yielding*.

Several failure models have been developed in order to suit specific criteria. For example, sandstone fails in shear condition, while clay may fail due to plastic deformation (Aadnoy & Looyeh, 2011). Known failure criteria are the Rankine, Tresca, Griffith and the St. Venon failure criterion. Nevertheless, two widely used models for shear and tensile failures are the Mohr-Coulomb Failure Criterion and the Von-Mises Failure Criterion respectively.

### 4.1.1. Mohr-Coulomb Failure Criterion

Mohr-Coulomb failure criterion is used for brittle materials that fails in both shear and normal stress. The criterion states "rock failure will take place when the shear stress across the failure plane is related to the corresponding normal stress" (Islam et al, 2010). The criterion is often used for materials that are stronger in compression than in tension, e.g. rock and concrete. By neglecting the intermediate principal stress, the criterion is defined by a linear approximation:

$$\tau = \tau_0 + \sigma \tan \phi$$

**Eq. 10 A linear approximation of Mohr-Coulomb Criterion**

Where $\tau$ is shear stress, $\tau_0$ is cohesive strength, $\phi$ is the angle of internal friction, and $\sigma$ is the effective normal stress acting on the grains. In drilling, the angle of internal friction, equals the angle of inclination of a surface sufficient to cause sliding of material down the surface (Jaeger, Cook and Zimmerman, 2007). An envelope of Mohr's circles represents the basis of the Mohr-Coulomb criterion, and the linear line (starting with $\tau_0$) was given by Eq. 10. This is also illustrated in the following figure:

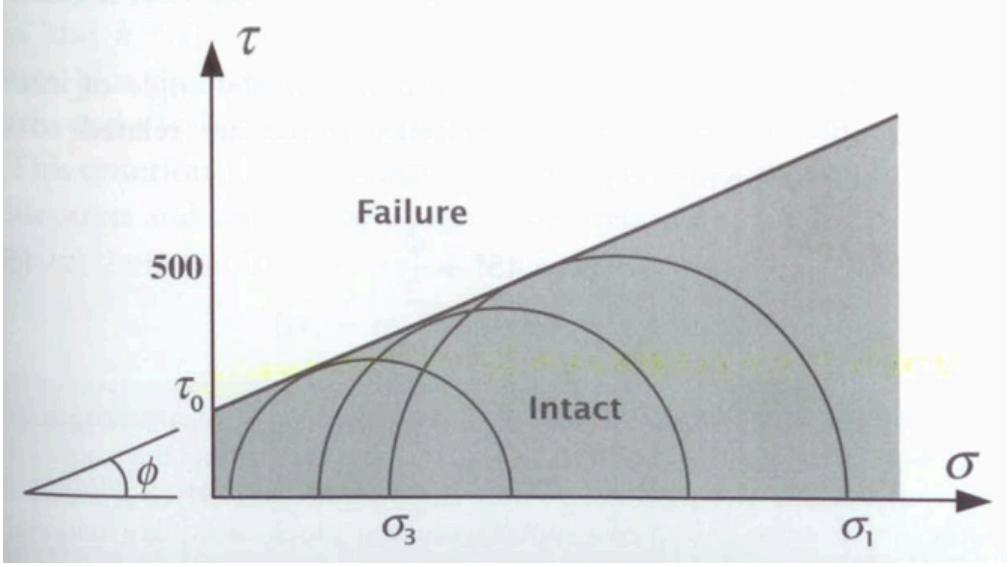


**Figure 9 Mohr-Coulomb failure criterion (Aadnoy & Looyeh 2011, p. 55, fig. 5.2)**

As the above figure indicates, the rock is intact if the relationship between stress and strain is *below* the line. The rock will fail in shear if the principal stresses are such that circle touches the failure line. If one of the Mohr's circles is above the failure line, the rock will fail. The circles are given by an individual triaxial test ($\sigma_1 > \sigma_2 = \sigma_3$), hence why the Mohr-Coulomb criterion has been used to represent rock failure under the polyaxial stress state ($\sigma_1 > \sigma_2 > \sigma_3$) (Islam et al, 2010). A triaxial test condition means that there are pressures exerted from top, bottom and sideways.

### 4.1.2. **Von Mises Failure Criterion**

The Von Mises failure criterion is one of the most reliable criteria used for ductile failure. Yielding begin when the distortional energy density (DED) at a point equals DED at failure. It relies on the second deviatoric invariant and the effective average stress, assuming triaxial test condition (Aadnoy & Looyeh, 2010). The second deviatoric invariant is defined as:

$$\sqrt{J_2} = \frac{1}{\sqrt{3}}(\sigma_1 - \sigma_3)$$

**Eq. 11 Second deviatoric invariant**

Effective average stress is defined as the average stress minus pore pressure:

$$\sigma_m - P_0 = \frac{1}{3}(\sigma_1 + 2\sigma_3) - P_0$$

**Eq. 12 Effective average stress**

These two equations are plotted towards each other, and forms two regions, similar to the Mohr-Coulomb's failure model. The area below the curve is *safe* (rock intact), while the area above the line is an unstable mode, and will cause failure.

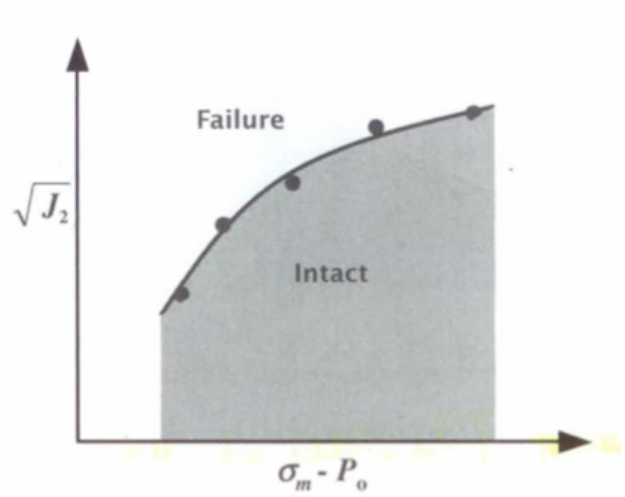


**Figure 10 Von-Mises Failure Criterion (Aadnoy & Looyeh, 2011, p. 55, fig 5.1)**

These criteria are not fixed, as they may be affected by several mechanisms. For example, Jaeger, Cook and Zimmerman (2007) proposed that pore fluid (water, oil, gas) could affect rock failure either by the mechanical effect of pore pressure, or by chemical interaction between the rock and fluid. The mechanical effect is due to pore pressure acting *outward* from its pore space, and would act like a tensile stress. Failure in soil would then be controlled by the effective stresses, which is principal stress minus pore fluid pressure:

$$\sigma'_i = \sigma_i - P$$

**Eq. 13 Effective stresses**

$\sigma_i$ is the denote for the principal stresses, $\sigma_1$, $\sigma_2$ and $\sigma_3$. By replacing the effective stresses, $\sigma_i$', with stresses, $\sigma_i$, in Mohr's diagram, the circles will be shifted towards the failure line. If pore pressure is increased sufficiently, the rock may fail due to the absence of pore pressure in the "safe" in-situ stress state ($\sigma_i$).

A chemical influence on rock failure is fluids interacting with one another. For example, the interaction between quartz-rich rocks and water has proven that the rocks' strength decreases (Jaeger, Price, Rutter and Parate, as cited in Jaeger, Cook and Zimmerman, 2007). A way of detecting irregularities in the borehole during drilling is to combine the current mud density towards annular pressure drop, which is defined by the effective density, *equivalent circulating density* (ECD).

### 4.2. Equivalent Circulating Density

ECD management is essential, as exploration into harsher and challenging environments requires accurate interpretation and control of pressure variation downhole. Knowledge of accurate down hole temperature, and precise leak-off tests and/or formation integrity tests have an essential role in ECD management, as they will determine its efficiency by operating within the safe pressure window (Rezmer-Cooper et al. 2000). Effective ECD management requires real time annular pressure supervision; hence rig safety is improved due to the detection of gas and water influxes. Pressure data can also be used to anticipate trends in ECD, hence avoiding drilling problems before they worsen into serious events (Aadnoy et al. 2009). ECD is calculated by the following equation:

$$ECD = d + \frac{P}{0.052 * TDV}$$

**Eq. 14 ECD**

Where d is the mud weight [ppg], P is the pressure drop [psi] and TDV is the true vertical depth. When a well is not circulating, there is no frictional pressure loss, thus

mud density variations is only influenced by thermal expansion or compression. This "pressure-temperature-density" behaviour is defined by the *equivalent static density*, ESD.

### 4.2.1. **Equivalent Static Density**

A study by Kaarstad and Aadnoy (1999), demonstrates the variations of ESD. For an offshore well (including input energy from mud pumping system and rotation of drillstring), the following density profiles was established:

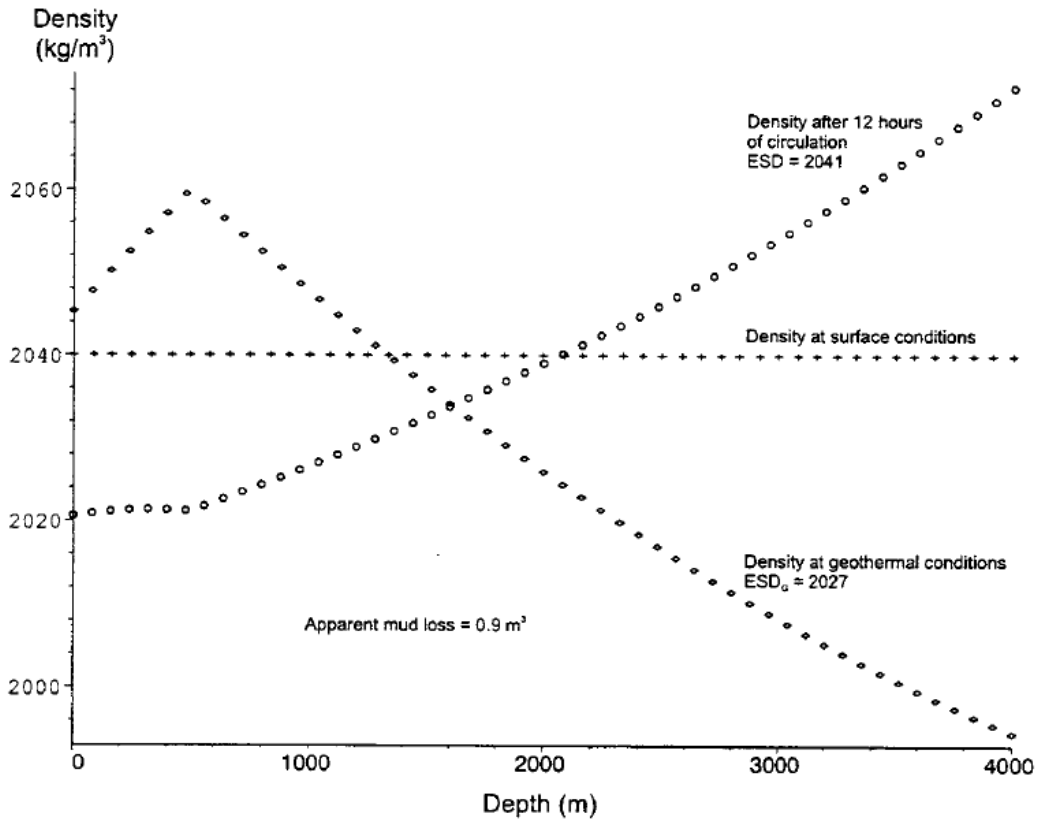


**Figure 11 Density profiles for an offshore well**

The figure shows density profiles at surface condition, at geothermal conditions, and during circulation. The circulating density increases with time since circulation causes cooling in the well's lower section and heating in the upper section. The equivalent density often stabilizes within 12 hours of circulation, although this is strongly dependent on the circulation rate. Wellbore cooling escalate at higher rates, hence the equivalent density will stabilize quicker and at a higher value. For the study given in figure above, circulating for 12 hours caused an increase in ESD of 0,014 s.g.

However, the consequential change in ESD will depend on mud properties. ESD are also influenced by other factors, especially water depth and mud flow rate. If drilling commences, friction pressure is added, and ECD will be even higher. Consequently, drilling induce fractures may occur.

# 5. Fracture classification

Stress has proven to be a determinant factor in a reservoir field as it influences fracture orientation, permeability around borehole, density, and distribution. This chapter will explain the definition of fractures, its process and interpretation of image logging, and at last, how to determine the fracture gradient. The subject of drilling-induced fractures will be emphasized.

## 5.1. Definition and types of fractures

According to Ma et al. (1993, p.1), a fracture is defined as ”any break or physical discontinuity in a rock caused by stresses exceeding the rock’s strength”. Three types of fractures may occur in the formation. These are natural fractures, induced fractures and hydraulic fractures. Natural fractures exist in the formation before drilling occurs, and drilling-induced fractures (as the name indicate) are a result of stress relief or rock strength failure caused by drilling. The third type of fracturing, hydraulic fracturing, takes place when the fluid pressure inside the rock exceeds the smallest principal stress plus the tensile strength of the rock. That is, fracture wings will develop perpendicularly to the least principal stress. This is why the fracture often propagates in a vertical direction since the smallest principal stress usually lies in the horizontal direction. Drilling induced fractures and hydraulic fractures have also a tendency to occur together due to high mud weight (which is optimized to give a high drilling rate) (Ma et al. 1993). The thesis will explain in detail how to distinguish between the different fractures in the chapter of borehole image logging tools.

Fractures are classified as either faults or joints, where the latter are the most common type of geological structure. Joints are defined as “cracks or fractures in rock along which there has been little or no transverse displacement” (as cited in Jaeger, Cook and Zimmerman, 2007). They are important in rock mechanics as they divide rock mass into different parts, hence cause sliding along the joint surfaces. Consequently,

they also provide paths for fluids to flow. Faults are a fracture surface that leaves displacement relative to one another, parallel to the fracture (Ma et al, 1993). Usually, they are approximately planar, so they provide important planes on which sliding can take place.

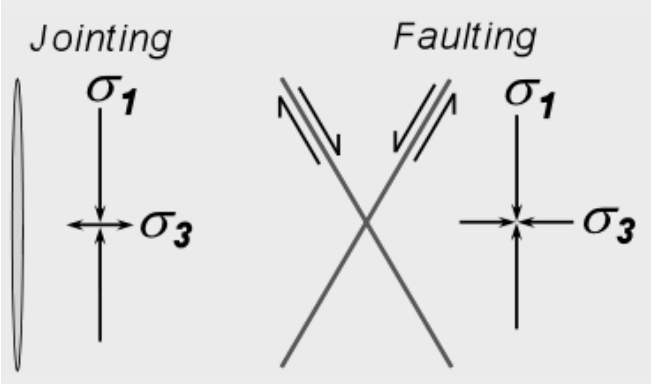

**Figure 12 Joint vs. Fault (Naturalfractures.com)**

### 5.2. Fracturing process

The fracturing process consists of five "events", which eventually leads to loss of circulation (Aadnoy et al. 2008). The process is illustrated in Figure 13. The first event is the *filter cake formation*. A filter cake is formatted due to small filtration loss on the borehole wall and is thickened by the following mudflow. The second event is *fracture initiation*. The filtrate cake is in place, but the hoop stress has changed from compression to tension due to increased pressure. The in-situ stresses resist the pressure, although fracturing will start at the critical pressure. In the third event, the fracture trace will widen if pressure is amplified, thus *fracture growth*. As seen from the figure, a stress bridge is formed, so the filter cake would still be intact. The stress bridge can be compared to a rock road bridge; higher top load increases compressive forces inside the curvature. The mechanical strength of the filter cake particles will therefore prevent the bridge from collapsing. This stress bridge also represents the plastic part of the elastoplastic model that will be explained later. The fourth event is *further fracture growth*. The stress bridge will then expand and becomes thinner due to further pressure increase. The last event is when the filter cake cannot resist the pressure and consequently collapses (*filter cake collapses*). The yield strength of the particles is then exceeded and leads to the adverse event of mud-loss towards the formation.

| Event | Fig. | Main Controlling Parameters |
|---|---|---|
| Filter-cake formation | 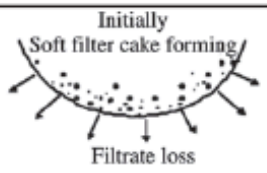 | Filtrate loss |
| Fracture initiation | 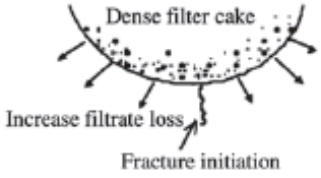 | Filtrate loss, stress |
| Fracture growth | 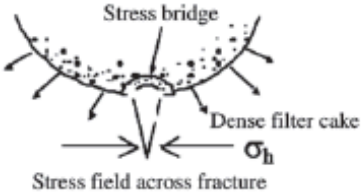 | Bridge stress, rock stress |
| Further fracture growth | 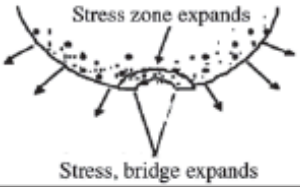 | Bridge/rock stress, particle strength |
| Filter-cake collapse | 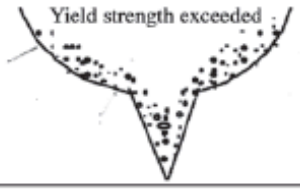 | Particle strength |

**Figure 13 Description of the fracturing process.**

### 5.3. Fracture interpretation from image log

One often assumes that the three principal stresses are oriented vertically or horizontally, all though this is not the reality. The only known way to determine the real orientation of the in-situ stress field (that also accounts for faults and folds) is to use an image log that reveals the fractures on the borehole wall (Tingay, Reinecker & Muller, 2008). From the figure below, two patterns will emerge whether the in-situ stresses acts normal to and along the borehole axis (a), or not normal to and non-axial to the wellbore (b).

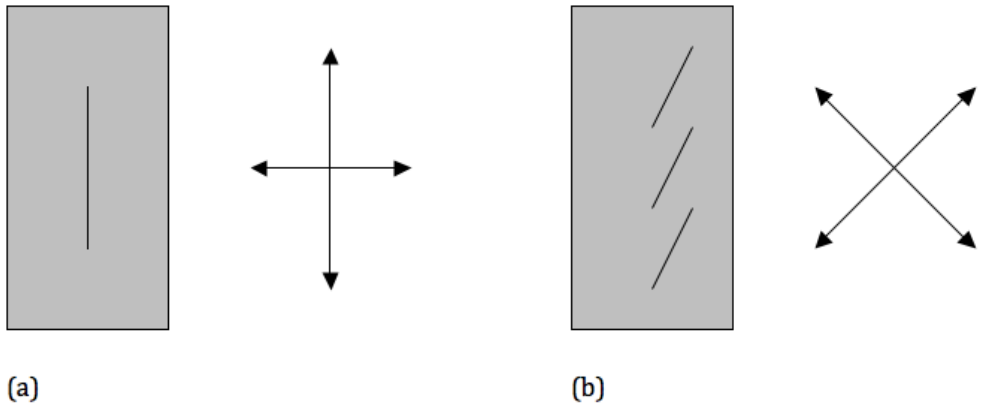


**Figure 14 Fracture patterns: (a) tensile fracture, vertical hole, (b) tensile fracture, deviated hole**

For figure (a), most shear stresses vanish since the fractures extend along the axis. Failure occurs at θ=0° and assuming $\sigma_y < \sigma_x$, the critical fracturing pressure becomes:

$$P_{wf} = 3\sigma_y - \sigma_x - P_o$$

**Eq. 15 Fracture pressure in a vertical hole (Aadnoy and Bell, 1998)**

This elastic model is used in normalizing data and establishing correlation. The fracture pressure will be parallel to the axis, as shown in Figure 14a, because the tangential stress will be the least principal stress. The shear stress component, $\tau_{\theta z}$, in (b) will arise due to the different orientation, consequently forming an en echelon pattern. This pattern is also evident in the image log that will be elaborated later in the thesis. The fracturing pressure in this case will be:

$$P_w = 3\sigma_y - \sigma_x - P_o - \tau_{\theta z}^{2/(\sigma_x - P_o)}$$

**Eq. 16 Fracture pressure for inclined borehole**

The en echelon pattern, demonstrated in Figure 14b above, represents an angle beta, β (Aadnoy, 1990):

$$\beta = \cos^{-1} \frac{\tau_{\theta z}}{\left[\left(\sigma'_\theta - \sigma'_3\right)^2 + \tau_{\theta z}^2\right]^{1/2}}$$

**Eq. 17 Inclination angle in a inclined borehole**

This angle often extends less than 30° around the circumference of the borehole.

### 5.4. Fracture gradient

A fracture pressure curve must always be presented for a well so that the driller knows which pressure interval he or she must be in-between, in addition to determine the mud gradient (Aadnoy, 2010). There are several modelling techniques for establishing a fracture plot, but the most common method is from elastic theory and geotechnical models (Kaarstad & Aadnoy, 2008). However, *geotechnical models* are based on material properties, and basically concern the upper parts of the ground. These models build upon cavity and initial yielding theory, and have proven to over-predict the fracture pressure. Hence, these models will not be discussed further.

According to Aadnoy & Looyeh (2011) "formation fracture gradient is the pressure required to induce fractures in the rock formation at a given depth". The precision of the determination of the fracture gradient is therefore an important part of the well planning process as it ensures a safe drilling performance. The fracture gradient is given by the overburden weight and lateral stresses of the formation, and can be determined either by a direct method or an indirect method (Rabia, 1985, MacPherson & Berry, 1972). The *direct method* relies on an experimental approach, e.g. leak-off test, while the *indirect method* uses analytical models, which relies on stress analysis techniques to calculate the fracture gradient. There are several methods used in the industry, whereas "Matthews and Kelly Method*"* are often used for offshore wells, while the "Eaton Method" has proven to be the most accurate.

Generally, the fracture gradient will decrease with increasing water depth, and it is important to recognize that there is a significant uncertainty related to the pore pressure curves, which yet again will affect the other pressure curves. Furthermore, most of the *indirect* methods were developed on empirical data obtained in 1960's and 1970's, where there were less accessible data than in today's data assemblage.

### 5.4.1. **Direct Method**

The most conventional direct method in determine the magnitude of the fracture pressure capacity and in-situ minimum horizontal stress is by a *leak-off test* (LOT), also called a pressure integrity test. The LOT is performed by shutting off the well and pumping mud into the borehole. Pressure will then gradually increase, and at some point the fluid will enter the rock formation either through permeable paths or by fracturing the rock. This is called the *leak off point*, which is represented as point A in the figure below. This point is often cited as the minimum horizontal stress. The pressure decrease towards point B (formation break-down pressure) is a response to the increased volume adhered in point A. The total fracturing pressure is then determined by adding the leak off pressure to the hydrostatic pressure of the mud. Finally, a safety factor is applied.

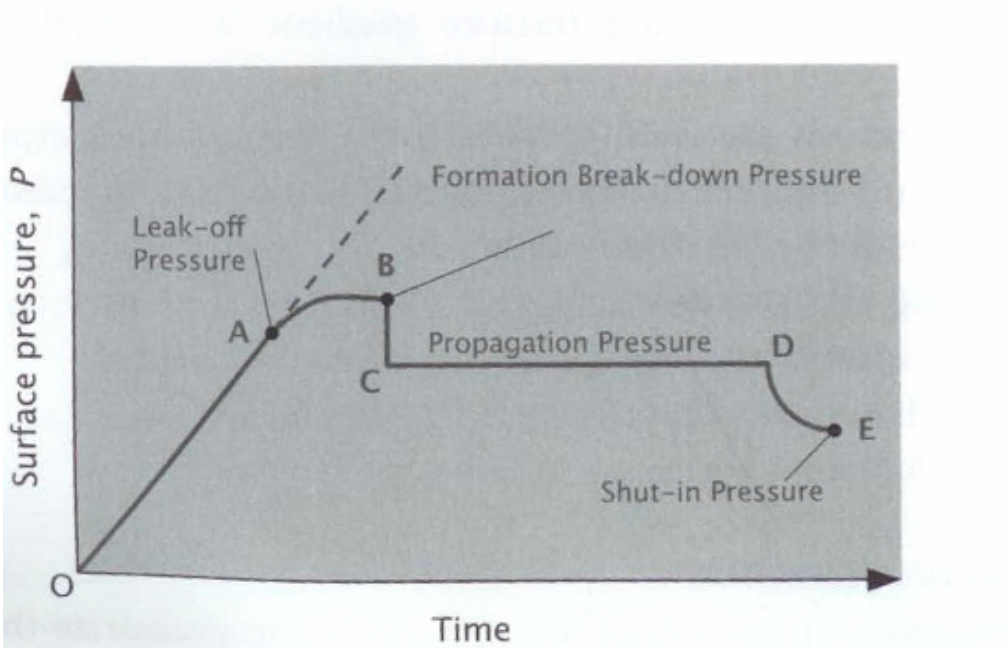


**Figure 15 Increment of Mud Pumped-In (Aadnoy & Looyeh, 2011, p. 136, fig. 9.3)**

Moreover, the formation breakdown pressure (B) is the final pressure that one establishes before determine reservoir treatment parameters (e.g. type of mud composition with regards to particle size and distribution). The propagation pressure (C-D) is close to the minimum in-situ stresses, so it should serve the basis for safe well design since a fracture will propagate when the pressure exceeds its minimum horizontal stress (Alberty & McLean, 2001). At last, the shut-in pressure (E) represents the pressure on top of the wellbore when it is closed. This pressure may be zero, though the well is then considered to be dead. The stress profile is made when

leak off data has been obtained. If estimation of the horizontal minimum stress is the primary purpose of the test, an *extended* LOT is more accurate, as the fracture re-opening pressure can be extracted from the test.

### 5.4.2. **Indirect Method**

The *Eaton method* is the most accurate indirect method used in determination of formation fracturing gradient, as it considers overburden pressure and the variation of Poisson's ratio with respect to depth (Aadnoy & Looyeh, 2011). This method is represented by the following equation:

$$G_f = \left(\frac{\upsilon}{1-\upsilon}\right)\left(\frac{\sigma_v}{d} - \frac{P_o}{d}\right) + \frac{P_o}{d}$$

**Eq. 18 Eaton equation**

Where $G_f$ represent the formation fracture gradient and the minimum calculated value, $d$ is the formation depth, and $\upsilon$ is Poisson's ratio.

As previously described, Matthews and Kelly Method are often used for offshore wells, typically for the North Sea and the Gulf of Mexico. This method uses the following equation:

$$G_f = f_e\left(\frac{\sigma_v}{d} - \frac{P_o}{d}\right) + \frac{P_o}{d}$$

**Eq. 19 Matthews and Kelly**

Where $f_e$ is the effective stress coefficient and is found from actual fracture data of a well nearby. This method is less accurate than the Eaton method.

So far, the processes and mechanisms behind fracturing have been given throughout the thesis. Research has been conducted over the last two decades in the attempt to find the exact causes of drilling induced fractures. The next chapter will describe those mechanisms that are seen most relevant in the determination of the fracture gradient.

# 6. The new fracturing model

As explained in prior chapters, several factors are interacting in the fracturing process. Causes of drilling-induced fractures are similar to those occurring naturally, but are essentially closely related to the in-situ stress condition (Zoback 1989). Simply put, the stress field of the environments has to overcome the fracture gradient in the rock.

A new model, first proposed in 2004 by Aadnoy and Belayneh, called the *elastoplastic model*, was similar to the elastic model, only a plasticity term, $P_y$, was added:

$$P_{wf} = 3\sigma_h - \sigma_H - P_o + P_y$$

**Eq. 20 Fracture model including plasticity**

This equation allowed for higher mud pressure even if the in-situ stress state was low due to the controlling plastic barrier. This plasticity term was also mentioned earlier in relation to formation of the stress bridge. Further on, the model evolved by including on the effect of Poisson's ratio, load history and temperature effect.

## 6.1. Effect of Poisson's Ratio

Aadnoy and Belayneh introduced the effect of Poisson's ratio to their model in 2009 since the old model under-predicted the fracturing pressure. Poisson's ratio arises due to tension in tangential direction caused by the load in the radial direction. The near wellbore stresses are still principal when borehole pressure is equal to the in-situ stresses. But when the mud gradient is introduced, the effect of Poisson's ratio arises on the stresses. By assuming principal stress state of $\sigma_v$, $\sigma_h$, and $\sigma_H$, the fracture pressure then becomes:

$$P_{wf} = \frac{(1+\upsilon)(1-\upsilon^2)}{3\upsilon(1-2\upsilon)+(1+\upsilon)^2}(3\sigma_h - \sigma_H - 2P_o) + P_o$$

**Eq. 21 Fracture pressure including Poisson's ratio**

The scaling factor at the beginning of the equation defines the contribution of Poisson's effect, and is defined as $K_{S1}$:

$$K_{S1} = \frac{(1+\upsilon)(1-\upsilon^2)}{3\upsilon(1-2\upsilon)+(1+\upsilon)^2}$$

**Eq. 22 Poisson's ratio scaling factor**

Typical ranges of Poisson's ratio for common lithologies are the following (Alberty & McLean, 2001):

**Table 3 Poisson's Ratio for common lithologies**

| Lithology | Poisson's Ratio |
|---|---|
| Sand | 0.10-0.22 |
| Silt | 0.15-0.30 |
| Carbonates | 0.20-0.35 |
| Shale | 0.22-0.48 |
| Salt | 0.45-0.50 |

### 6.2. Load History

The new model also includes load history, which requires the establishment of initial conditions. The figure below represents load history of a borehole. One can see how pressure responds to the different operations that the wellbore is being exposed to during the time of drilling, until a LOT test is performed:

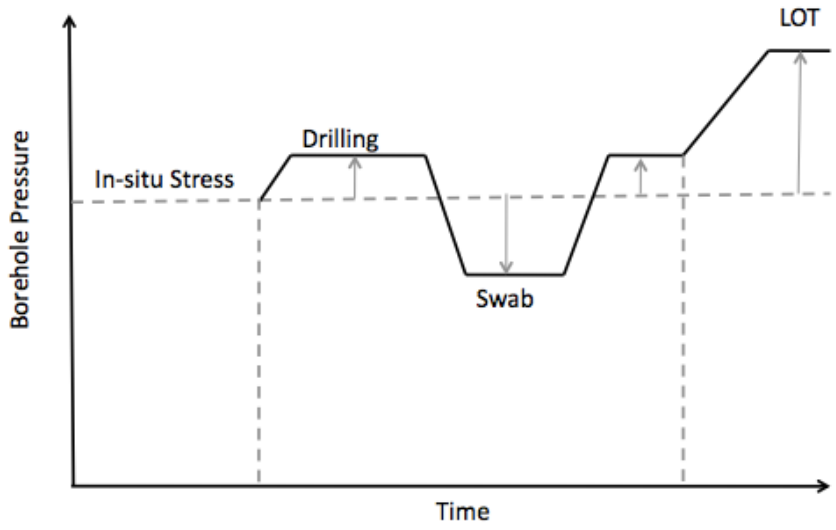


**Figure 16 Load history (redrawn from Aadnoy & Belayneh, 2009)**

The arrows display the longitude at which the pressure deviates from its original in-situ stresses. One assume that a principal stress state exist in the rock formation before it is disturbed, and that the stresses are transformed in space if the borehole deviates from the principal stress state. For example, in a vertical borehole, $\sigma_v$ will be largest of the principal stress, fracturing will then occur in the direction of $\sigma_H$. Then, the initial condition will be defined by $\sigma_h$, which is acting normal to $\sigma_H$.

Thereafter, swabbing reduces pressure in the wellbore due to moving pipe. Swabbing is done by sealing off the wellbore with rubber-cupped seals or wireline tools. It is considered harmful as it may lead to kick or wellbore instabilities since reservoir fluids can flow into the wellbore and towards surface, if pressure is sufficiently reduced (glossary.oilfield.slb.com, 2012). In relation to swabbing, *surge* can also reduce pressure inside the wellbore due to e.g. high tripping rate. One can visualize surge to be the same as pulling your boot out of mud too fast. From experience, you will probably remember that it gets stuck, and you have to pull your leg slowly in order to get it out of the mud. Swabbing and surge control in wellbore is important as they can cause costly drilling problems such as fracturing (resulting in lost circulation), fluid influx (resulting in kicks), formation breakdown, and blowouts (Srivastav et al. 2012).

The fracturing pressure will differ whether an isotropic loading (equal normal stresses) or an anisotropic loading (two distinct normal stresses) acts on the borehole wall (Aadnoy and Looyeh, 2011). For an isotropic loading, the initial stress condition is equal to the pre-existing in-situ stress, σ, and the fracturing pressure becomes:

$$P_{wf} = \sigma + P_0 + K_{S1}\left(\sigma - 2P_0\right)$$

**Eq. 23 Fracturing pressure at initial state for an isotropic case**

As seen from the equation, stress does not have any denotes here since the stresses around the borehole are assumed to be equal. It is however very rare that a field has an isotropic stress state.

For the conventional case where the two horizontal stresses have different magnitudes, i.e. *anisotropic* loading, the position of fracture initiation will rise in the direction of $\sigma_H$. Accordingly, the fracturing pressure becomes:

$$P_{wf} = \sigma_H + P_0 + 2K_{S1}\left(\frac{3}{2}\sigma_h - \sigma_H - P_0\right)$$

**Eq. 24 Fracture pressure at initial state for an anisotropic case**

### 6.3. Temperature Effect

In early research, the effect of temperature was usually neglected due to simplification of the models, and lack of technology. Nevertheless, temperature has proven to have a significant effect on the fracture pressure (Maury & Guenot, 1995, Gonzales et al. 2004, Aadnoy and Looyeh, 2011). This was also emphasized by Aadnoy and Belayneh (2009), as they concluded that heating increased the fracturing initiation pressure and cooling decreased it given that expansion and/or contraction changed the hoop stress. The following temperature contribution is therefore significant in the calculation of the critical fracture gradient:

$$P_{wf} = K_{S2} * E\alpha\Delta\mathrm{T}$$

**Eq. 25 Fracture pressure including temperature effect**

Where E is the elastic modulus [Pa], $\alpha$ is the coefficient of linear thermal expansion [$°C^{-1}$] and is typically around $1{,}5*10^{-5}$ / °C (Fjaer et al. 2008 p.388). $\Delta T$ is the temperature change from initial condition, $T_0$ [°C], and $K_{S2}$ is the scaling factor for temperature effect, defined as:

$$K_{S2} = \frac{(1+\upsilon)^2}{3\upsilon(1-2\upsilon)+(1+\upsilon)^2}$$

**Eq. 26 Scaling factor for temperature effect in terms of Poisson's ratio**

The coefficient of linear thermal expansion is strain associated with 1/°C temperature change (also given in 1/°K and 1/°F), and assumes an isotropic rock. If rock is subjected to both change in temperature and an applied stress state, the resulting strain will be the sum of thermal strain and stress induced strain (Jaeger, Cook and Zimmerman, 2007, p.198-204). For this reason an increase in temperature (heating → positive thermal strain) gives an increase in bulk volume, and a temperature reduction (cooling → negative thermal strain) will cause the bulk volume to decrease. This coefficient's value will differentiate depending on the type of rock and material, and the thesis will elucidate thermal effect in depth later on.

### 6.4. The complete general fracturing model

Taken the above-discussed sections into account, the new *general* equation for fracture pressure becomes (Aadnoy & Belayneh, 2009, Aadnoy & Looyeh, 2011 p. 228):

$$P_{wf} = \sigma_y + \frac{2(1+\upsilon)(1-\upsilon)}{3\upsilon(1-2\upsilon)+(1+\upsilon)^2}\left(\frac{3}{2}\sigma_x - \sigma_y - P_0\right) + P_0 + \frac{(1+\upsilon)^2}{3\upsilon(1-2\upsilon)+(1+\upsilon)^2}\mathrm{E}\alpha(T-T_0) + \frac{2Y}{\sqrt{3}}\ln\left(1+\frac{t}{a}\right)$$

**Eq. 27 New general fracture model**

The in-situ stresses is referred as (x,y) coordinate system since they have been transformed in space. $\sigma_x$ is the least normal stress acting on the borehole, t is the thickness of the filtercake [m], and *a* equals borehole radius [m]. Y is the nomenclature for yield strength.

The last element of the equation represents the elastoplastic barrier that is caused by the mud cake due to its plastic behaviour. Nevertheless, there are no present methods to compute this magnitude, thus its usually ignored. Notice that the complete model will differentiate regarding the presence/assumption of:

- an isotropic stress loading
- an anisotropic stress loading
- a penetrating situation (no communication of wellbore fluid)

$$\Delta P = P_{wf} - Po = 0$$

- a non-penetrating situation (communication of wellbore fluids)

$$P_{wf} > Po$$

## 7. Borehole image tool

Borehole image log tool was first introduced as the Borehole Televiewer (BHTV) in the late 1960's (Zemanek et al. 1969). Kulander, Dean & Ward (1990), and Lorenz, Finley & Warpinski (1990) further on conducted several core analyses in order to document drilling induced fracturing. The borehole image log gives a visual perception of the down-hole environment in order to allocate an evaluation of the formation, as for example fractures and borehole breakouts. The tool is essential in drilling technology, especially since it is (as of today) the only tool that can observe and distinguish drilling induced fractures from natural fractures (Aadnoy et al. 2009). Furthermore, it is also important regarding the search for new oil in HPHT wells and deepwater wells as it aids the planning process of new wellbores.

Imaging tools today falls predominantly under two categories as either acoustic or resistive image tools, and the latter is the most conventional. It is, however, important to highlight that these tools *in combination* with other measurements facilitate an enhanced complete picture of the borehole condition. Other measurement tools can be surface dynamics measurements (e.g. torque, pump pressure, hook load), mud-logging measurements, and other MWD (measurements while drilling) e.g. annular and internal pressure. One example, is the combination of annular pressure

measurement, real-time LWD (logging while drilling) and resistivity-at-the-bit tool, which together provide important information regarding:

- Identifying drilling hazards
- Monitor formation failure and invasion
- Enhance ECD management
- Improve petrophysical and geological interpretation
- Optimization of drilling operations by aid in the selection of remedial methods

### 7.1. The resistivity image log

The resistivity image log takes electrode resistivity measurements in wells using a water-based mud or conductive mud. It consist of four or six calliper arms which then again have one or two pads containing several resistivity buttons (Tingay, Reinecker & Muller, 2008). These resistivity buttons allows high-resolution images of the borehole wall as well as providing information about borehole diameter and geometry.

According to Aadnoy et al. (2009), the highest resolution images available using LWD technology is recorded at resistivity-at-the-bit tool. It provides information from three different measurements:

**Table 4 Resistivity-at-the-bit tool measurements**

| | |
|---|---|
| *Bit* resistivity | Measures resistivity around bit with a vertical resolution vertical to its length. |
| *Ring* resistivity | Measures approximately 3 ft above the lower end of the tool, and gives accurate high-resolution measurements with a diameter of approximately 22 inches. |
| *Three button* | Focused, lateral measurements that records azimuth data at 1, 3 and 5 inches depth of investigation. |

There are a variety of resistivity tools available, the most common are the Formation Micro Imager (FMI), Formation Micro Scanner (FMS) and Oil-Based Micro Imager (OBMI), all from Schlumberger. Borehole breakouts will appear as broad, parallel, poorly resolved conductive zones because there will then be poor contact between the

wellbore wall and the tool pads. The drilling induced fractures appears as pair of narrow, well defined conductive features. This is also seen in the picture below (Tingay, Reinecker & Muller, 2008).

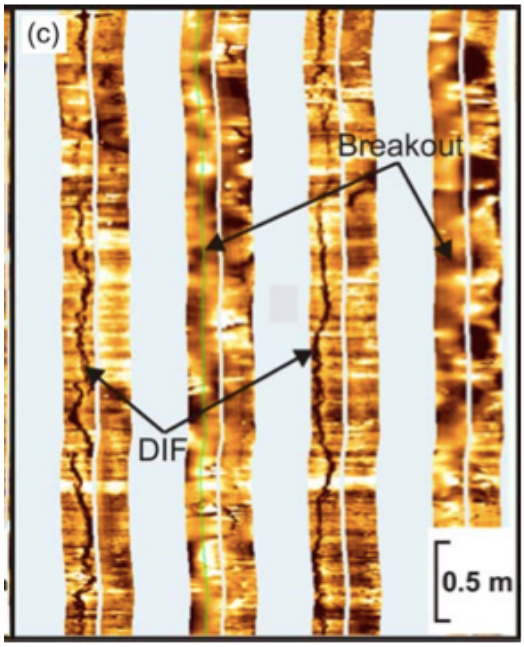

**Figure 17 Breakouts and drilling induced fractures from a FMI.**

DIF is the abbreviation for drilling induced fractures, and is oriented 045°N and 225°N in the figure above. Advantages for the resistive image log is its cost efficiency due to high-quality images although logging speed is high (548 m/hr to 1097 m/hr) (Li et al. 2009). However, the tool has limited borehole coverage, e.g. in a 7" hole, the limited image coverage will be around 40%. This is also seen as the grey stripes in the figure above. Another disadvantage is that the tool cannot distinguish between open fractures and "healed" fractures (cemented fractures), as they will give the same resistive response. The exception is when a conductive mineral (e.g. pyrite) is used in the cemented fracture because it will give a conductive response on the image log. An acoustic log will therefore be a relevant tool in the capability of differentiation between these fractures.

### 7.2. The acoustic image log

The acoustic log utilizes a rapidly rotating piezoelectric transducer (convert electrical energy to acoustic energy and conversely) to emit a focused high frequency sonic

pulse to the borehole wall (Asquith and Krygowski, 2004 p. 244, ndt-ed.org, 2012). The amplitude of the return echo and the total travel time of the sonic pulse are then recorded at several azimuths inside the wellbore at the desired logging depths. Some of the conventional tools regarding the acoustic log are the Borehole Televiewer (BHTV), Ultrasonic Borehole Imager (UBI), and Circumferential Borehole Imaging Log (CBIL). Borehole breakouts are found by using the borehole radius, as seen on the figure below. Drilling induced fractures are more difficult to interpret compared to the resistivity log as they are observed as zones with low amplitude and higher radius (see Figure 18b). Another disadvantage is the slow logging speed (91-152 m/hr), hence it is less cost effective (Li et al. 2009).

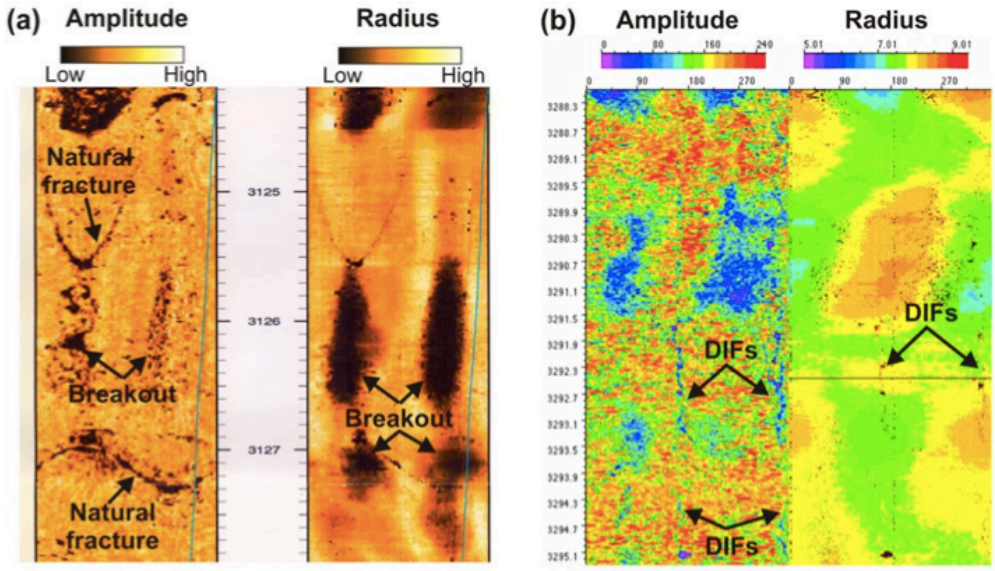


**Figure 18 Breakouts and DIFs from acoustic image log.**

### 7.3. Unconventional image logs

In addition to the two tools described above, *logging while drilling* (LWD) and *measure while drilling* (MWD) are also used in analysing borehole breakouts and drilling induced fractures. They provide information on bulk density and photoelectric factor (Pe) at a range of azimuths surrounding the wellbore. Photoelectric factor is a sensitive factor of mineralogy, hence improving matrix densities (e.g. porosity interpretation) (Asquith & Krygowski, 2004). The highest resolution images used in LWD are recorded in the *resistivity-at-the-bit* tool, and have been described earlier. The tool uses the Earth's magnetic field as a reference to determine its angular position when the drill string rotates. Hence, giving the tool the ability to make azimuth resistivity measurements. *Azimuth* direction is usually considered as degrees

towards the *magnetic north* (OilGasGlossary.com, 2012). Finally, optical imaging logging tool are also used in the interpretation of the wellbore wall. It utilizes a camera to image the wall directly.


**Figure 19 Fracture from downhole camera (Asquith and Krygowski, 2004)**

## 8. Temperature effect

An effect that has proved to have a significant influence on borehole stability is the temperature effect. This factor was often neglected in the early empirical and analytical models of borehole stability due to e.g. lack of information (poor temperature measurement tools), and simplifying assumptions (no energy supply from the hydraulic pump system, or friction between circulating fluid and casing). Additionally, many models were based on the application of onshore wells. Hence, cooling of fluid inside the riser down to seabed was not a consideration. Thermal effect has also proven to have a great impact on several decision makings regarding casing setting depth, determination of ECD, and composition of cement, drilling mud and annulus fluids (Kaarstad & Aadnoy 1997, Gonzales et al. 2004). The effect is not only important in the aspects involving drilling, but also in completion, production and injection. This paper focuses however on thermal effect regarding the drilling aspect since that is the occurrence of the drilling induced fractures.

The heat conduction is a slow and transient process as the temperature profile is affected by factors such as mud-in temperature, change in depth, rotation from drill string, and the hydraulic pump system (Kaarstad, 1999). Temperature is also in

transition in the tubular and annular fluid, as cold mud will enter the inside of the drillpipe, and being heated by contact with the pipe wall. The return mud will be exposed to both outside of the drillpipe as well as annulus. Accordingly, the inside and the outside of the pipe-wall will have distinct temperatures. This is also illustrated in the following figure (Kaarstad and Aadnoy, 1997). Another important aspect to the temperature effect is that cooling of the bottom occurs when circulation of wellbore fluids commences. Consequently, the temperature in mud return increases, causing a heat loss from the well. This cooling effect is strongly influenced by the flow rate and circulating time.

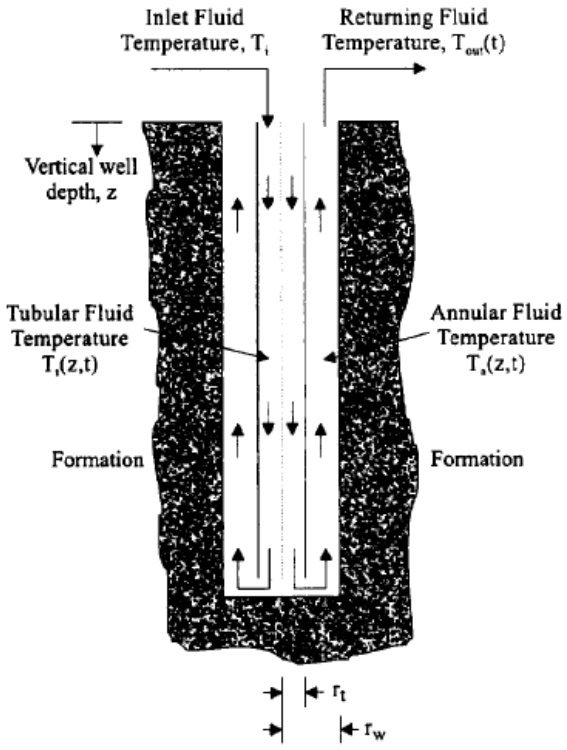


**Figure 20 Circulation system of fluid**

The well temperature is directly related to the initial temperature in the formation, which is called the *virgin formation temperature,* VFT. This temperature is important to be determined in order to analyse a well's PVT behaviour as well as it works as a reference temperature, e.g. determine the change of stress due to temperature (Kaarstad, 1999):

$$\sigma_T = \frac{E\alpha}{(1-\upsilon)}(T - T_0)$$

**Eq. 28 Change of stress due to temperature**

Where $T_0$ is the VFT. Note that this equation is also used in the new fracture model.

As previous stated the well temperature is also very sensitive to flow rate. When circulating the bottom hole, the fluid temperature often drops to a lower level, causing a cooling effect around the wellbore. This cooling effect will thereby influence the surrounding stresses, hence lower the effective fracture gradient and may cause failure (Hettema, Bostrøm and Lund, 2004). On the other hand, increasing the temperature effect (heating) will increase the fracture gradient, consequently resulting in a less likely tensile failure occurrence. Wellbore temperature may also fall due to other events. For example, the formation can alter a significant temperature reduction due to filtration loss in a high permeable zone.

### 8.1. Temperature profile in a well

The lifeblood of the drilling process is the drilling mud, and it will expand and extract as a reaction to variations in pressure and temperature. The thermal process is evident when mud is being pumped down to the drill-bit. The fluid is first exposed to cooling from the harsh North Sea climate and cold seawater, down to the seabed. The mud is subjected to heat due to contact with pipe wall and increasing depth (frictional forces). As the mud is pumped through the bit and returned, it is exposed both to the outside of pipe wall and annulus. Thus, the drillpipe works as a counter-current heat exchanger, where the mud temperature inside the drill-string is usually lower than the mud temperature in annulus. This is also illustrated by the figure[1] below, where annulus temperature, $T_a$, is higher than tubular temperature (inside temperature), $T_t$, (Kaarstad & Aadnoy, 1999):

[1] This profile only highlight the general interpretation

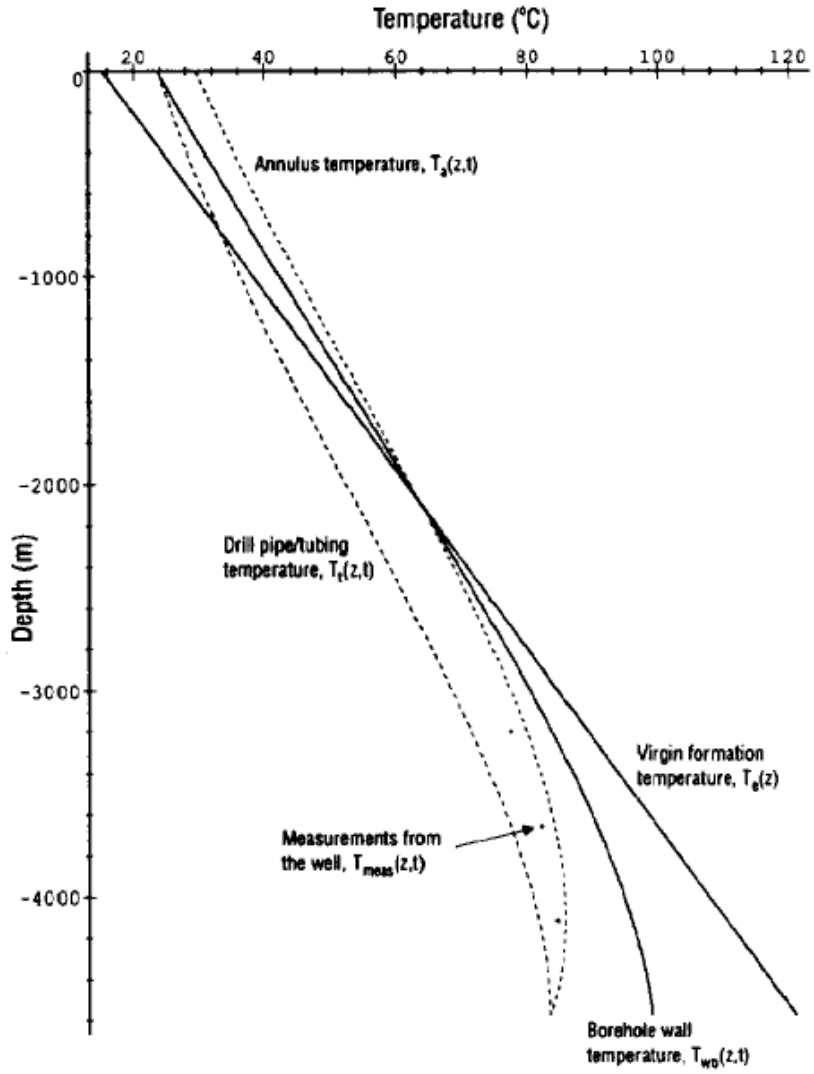


**Figure 21 Temperature profile for a well**

The mud-in temperature increases due to the increasingly mud pit temperature during drilling. In shut-in, the mud will expand and reduce its density since it will then gradually increase its temperature towards the geometrical temperature.

The following figure illustrates how circulation can affect the well temperature. Temperature behaviour (including input energy from rotation and pumping) for both mud and on borehole wall are demonstrated for two hours and six hours (Kaarstad & Aadnoy, 1999):

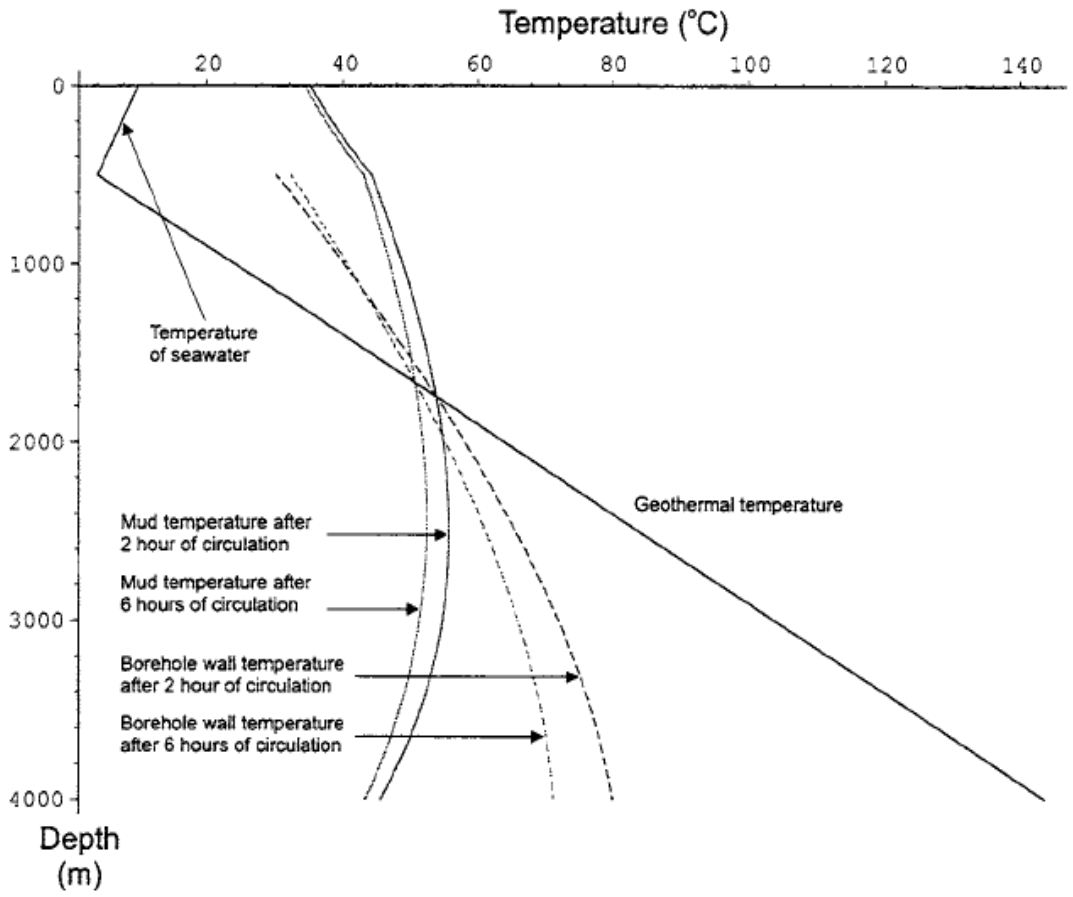


**Figure 22 Temperature change due to circulation**

Observation from the figure above shows that even though the mud experiences a relative "small" temperature reduction due to circulation, the borehole wall temperature encounters a considerably greater temperature change. This implies how sensitive the borehole wall temperature is towards temperature changes in mud temperature, which is an important observation regarding drilling induced fracturing. Many studies have demonstrated the importance of acknowledging thermal effect, as tensile failure has resulted in fluid loss. Some of them will be described in the followingsection.

### 8.2. Studies of temperature effect

Formation loss (caused by tensile failure) is a major issue for the drilling industry, and due to the formation's diversity, there would be different solutions regarding the various conditions and assumptions for the particular field. An example is a case study from the western desert in Egypt, which stated that drilling induced fracturing was only a problem for highly deviated wells (more than 55°- 60°). The paper concluded that drilling induced fractures were reduced by drilling close to the minimum horizontal stress direction (Van Steene et al. 2010). Another study by Hettema, Bostrom and Lund (2004) was conducted, as loss of circulation during drilling through cooled formations in the North Sea was a great issue. The mature fields had water injection wells as a part of their infill-drilling program, which caused the formation to cool, hence changed the in-situ stresses. The paper investigated the distance from the different wells, the effect of temperature in mud and seawater, and the near-wellbore thermal stresses. One of their conclusions was that injection of seawater in a near wellbore caused cooling of formation, hence loss of fluids in the wells that was drilled. Mud, which was warmer than the formation proved to be a time-dependent compressive contribution, and downhole pressure data confirmed that the cooling effect reduced the minimum stress, hence the fracture gradient. This conclusion is also supported in other papers (Perkins and Gonzales, 1981, 1985).

Another paper studied various factors that affected wellbore temperature in order to find a solution towards their problem of thermal induced fluid circulation losses (Gonzales et al. 2004). The factors that were explored were flow rate, temperature dependent LOT, mud temperature variations, circulation parameters, mud and cement properties, and the relation between mud and ECD. The study concluded with a strong correlation between wellbore temperature and loss of circulation, and encouraged for thermal management to control and manipulate the affecting factors to reduce the thermal effect on the borehole wall. Another important conclusion was that wellbore temperature influenced the result of a LOT. The difference between the geothermal static temperature and the wellbore's temperature could be the explanation of the differences in LOT-test result and the predicted effective fracture gradient. Gonzales et al. (2004) supported the conclusion that Hettema, Bostrom and Lund (2004) stated;

wellbore temperature contributes in rising and lowering the effective fracture gradient whether the wellbore temperature increases or reduces respectively.

Although these studies are prone towards a higher mud temperature, the solution may not be as simple as increasing the mud-in temperature. Chen and Ewy (2005) stated "heating the wellbore may result in more increase to pore pressure than to the hoop stress. Under this circumstance, heating the wellbore can reduce the effective hoop stress and consequently reduce the fracturing mud weight. It is also seen from this paper that collapse mud weights can first increase and then decrease with time when the wellbore is heated".

The general conclusions are to improve the accuracy of determination of anisotropy mechanical properties, and estimating the horizontal stresses, hence improving the pore pressure curves (Khan et al, 2012). Consequently, an improved prediction of the mud gradient is then obtained.

## 9. Well study

The Gjoa field lies approximately 63 km from the west coast of Norway, and the studied well was drilled in 1996. This well had great issues with mud loss during drilling, hence a thorough analysis was conducted by Eriksfiord (consulting company which specialize in geosciences) with e.g. image log, to analyse the well further. Several incidents of drilling induced fractures were observed along the borehole wall, although ECD pressure was stable during drilling.

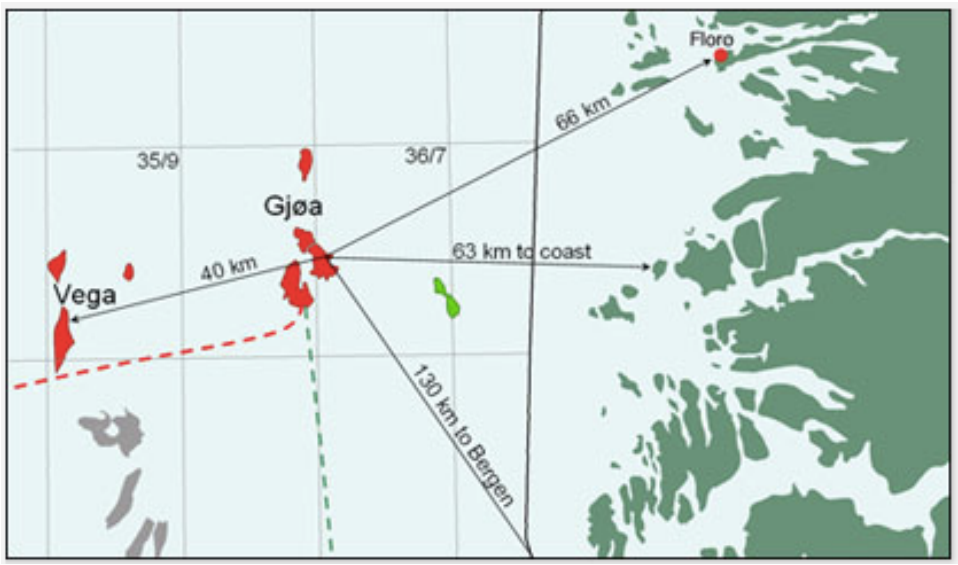


**Figure 23 Gjoa field (Statoil, 2009)**

The depth from mean sea level (MSL) to seabed was 380 m and true depth (TD) was 2841 mMD. The well was drilled in four sections and had an open-hole interval from 1256-2837 mMD. Maximum inclination was 8,8 degrees, and the reservoir consisted of mainly sandstone, siltstone and shale (npd.no, 2012). The well's hole diagram is also illustrated by figure below.

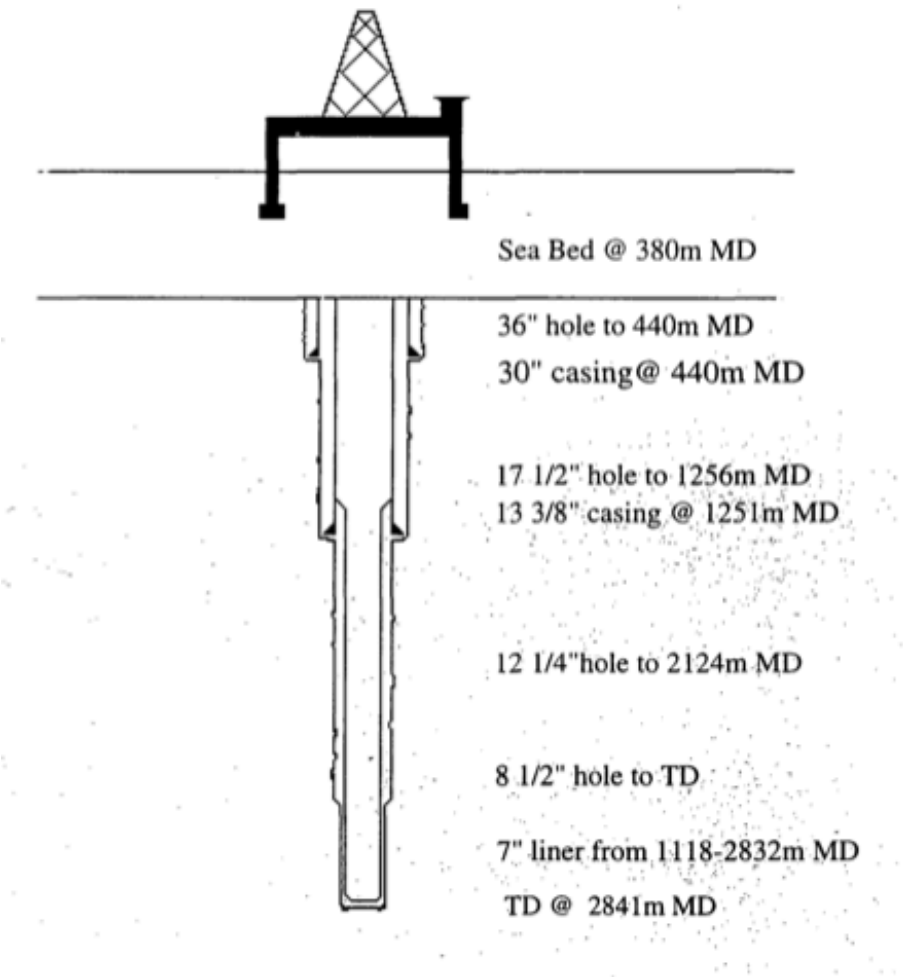


**Figure 24 Hole diagram**

A LOT was conducted at 1259 mMD with 1.20 SG mud in the hole. The formation was tested to leak of, and gave an equivalent mud weight of 1.46 SG. The following pressure diagram was obtained:

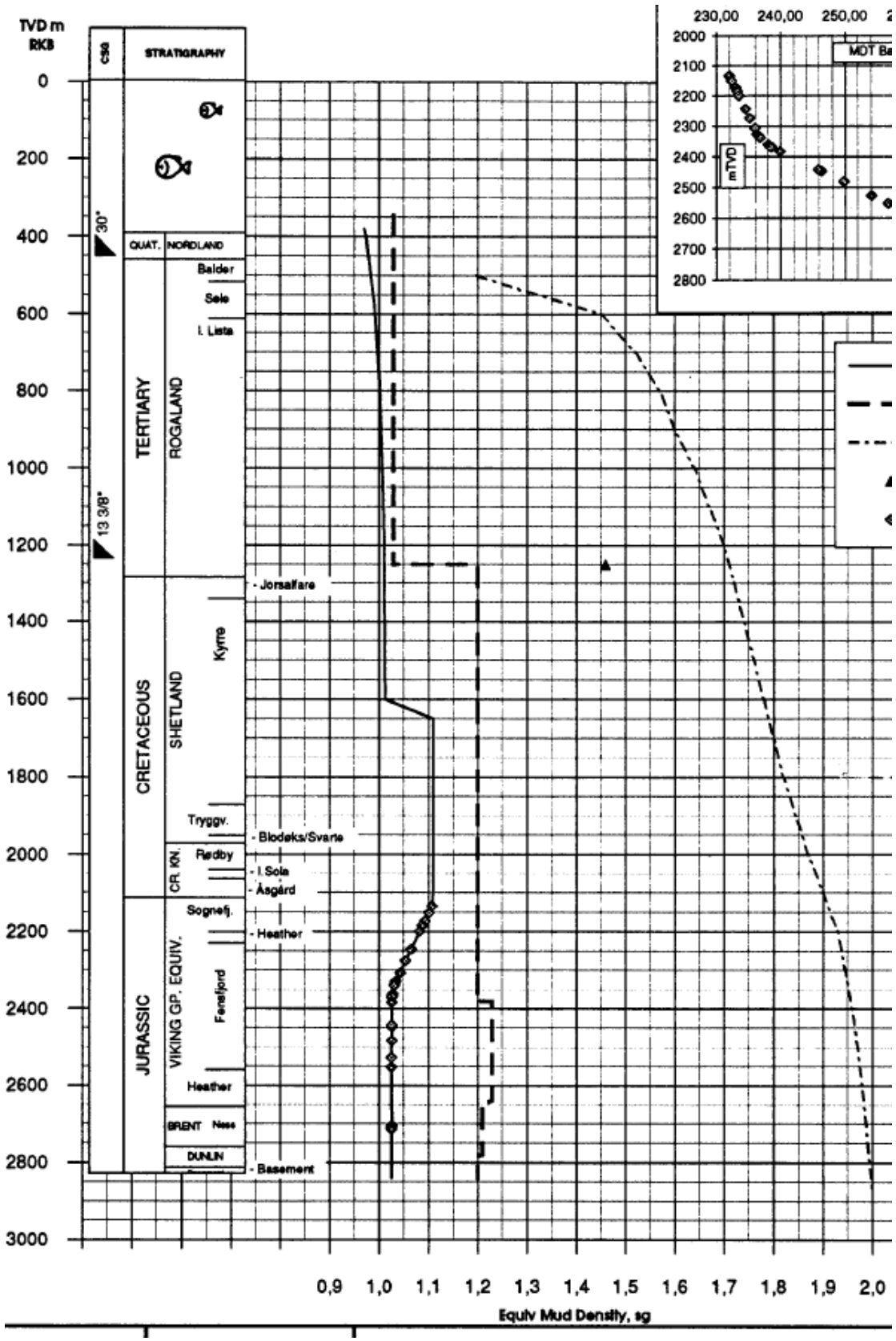


**Figure 25 Pressure diagram for the studied well**

The black line represents pore pressure, the heavy dashed line stapled mud pressure, and the thin dashed line represents overburden pressure gradient. The triangle in the middle of the diagram around 1200 mTDV represents the leak-off pressure. The points on the bottom of the pore pressure curve represent MDT data (modular formation dynamics tester), and will be discussed later.

## 9.1. Data acquisition

The following summarizes the most important information obtained from the reports in relation towards this study.

### 9.1.1. Eriksfiord well report

As explained in the beginning of the chapter, Eriksfiord conducted an analysis of the well, four years after drilling ceased. The main information was encountered from the FMI logged interval of 2121-2674 mMD:

- Maximum measured temperature was 71°C, so no chemical compaction took place due to the low temperature.
- A water-base drilling fluid with density of 1.21 g/cc was used.
- The well showed a partly complex fault and dip patterns.
- Maximum wellbore inclination was 8,8°
- Abundant fractures were encountered in the wellbore.
- Conductive fractures (natural open joints) were observed, and are most likely responsible for the mud loss in well.
- No breakouts were encountered.
- Hole conditions are generally in-gauge with smooth borehole wall.
- Overall image quality was good to very good.
- Drilling induced fractures were observed in two distinct zones: 1844 – 1958 mMD and 2340-2670 mMD.
- Poor image log quality from 2100 – 2400 m.
- Mud loss suggests communication between the drilling-induced fractures and the natural open joints, or even drilling-induced fractures propagating into the far-field stress regime.

- Drilling-induced fractures seemed to develop exclusively in the mudstones. However, tensile fractures were also found in cemented sandstone.

Furthermore, the report emphasizes the field's bedded formation. It has been established that a weakness in bedded rocks, may cause severe borehole collapse issues (Aadnoy et al. 2009[2]). A critical weakness in the rock strength properties is an angle between borehole and bedding of 10° to 30°. However, the maximum inclination of the studied well was 8,8°. In addition, this subject is more related towards shear failure, and will thus not be discussed further.

### 9.1.2. **Final well report**

There were some interesting observations from the final well report. The following tables highlight those of biggest interest (highlighted in bold) in regards to what may have initiated the drilling induced fractures.

**Table 5 Draft from daily well report**

| | | |
|---|---|---|
| Date | 09.09.1996 | |
| PP estimated [sg] | 1,10 | Mud weight [sg]: 1,20 |
| | | |
| Time | Description | |
| 22.00 | Circulating the hole clean | |
| 23.30 | Flow checked the well and pulled out of the hole from 2124 m to 1692 m. | |
| | **Due to swabbing further pulling out of the hole was stopped.** | |
| 23.59 | Ran back in the hole from 1692 m to 2124 m. | |
| | | |
| Date | 10.09.1996 | |
| PP estimated [sg] | 1,10 | Mud weight [sg]: 1,20 |
| | | |
| Time | Description | |
| 02.00 | **Circulated the well** | |
| 04.30 | Pulled out of the hole from 2124 m to 1251 m. | |
| 07.00 | Pulled out of the hole from 1251 m to 184 m. | |
| 09.00 | Pulled out of the hole with the bottom hole assembly. | |

Swabbing occurred in the interval where the drilling induced fractures were observed, additionally, the well was circulated for two and a half hour. Chapter 8 explained how

circulation effect borehole wall temperature. For example, it was demonstrated that circulation in a well from two hours to six hours decreased the borehole wall temperature as much as 10 degrees. The thesis has also explained that both swabbing and circulation can contribute to the cause of drilling induced fracturing due to reduction in pressure and temperature. Furthermore, the report described an ongoing process of coring (going in and out of the well in order to gather core samples) for four days. The next interesting observation in addition to a second occurrence of swabbing, is that the mud weight was higher than usual i.e. 1,24 sg. In spite of this, the ECD pressure was stable (in fact it was consistently vertical).

**Table 6 Draft from daily well report #2**

| | | |
|---|---|---|
| Date | 14.09.1996 | |
| PP estimated [sg] | 1,1 | Mud weight [sg] : **1,24** |
| Time | Description | |
| 19.00 | Spaced out the core barrel, dropped the ball and cut core no. 6 from 2275m to 2301 m before the core jammed. | |
| 20.00 | Circulated the hole for 10 minutes and pumped out of the hole from 2309 m to 2124 m due to **indication of swabbing** | |
| 21.00 | Flow checked the well, pumped slug and pulled out of the hole to 1251 m. | |
| 23.00 | Pulled out of the hole to 182 m. | |

In theory, these events can all contribute to the occurrence of drilling induced fractures observed in the interval of 2256 mMD to 2268 mMD from the image-log. The further events reported were mainly coring, reaming and logging.

### 9.2. Fracture interpretation from image log

As explained earlier, the FMI image log identified several fracture planes along the logged interval. Fracture planes are seen as bright and dark features in the image, and differentiates between natural resistive, conductive, and drilling induced fractures. Resistive fractures were defined as closed natural fracture planes, and are represented by the purple curves in the following figure (all figures are from Eriksfiord, 2010):

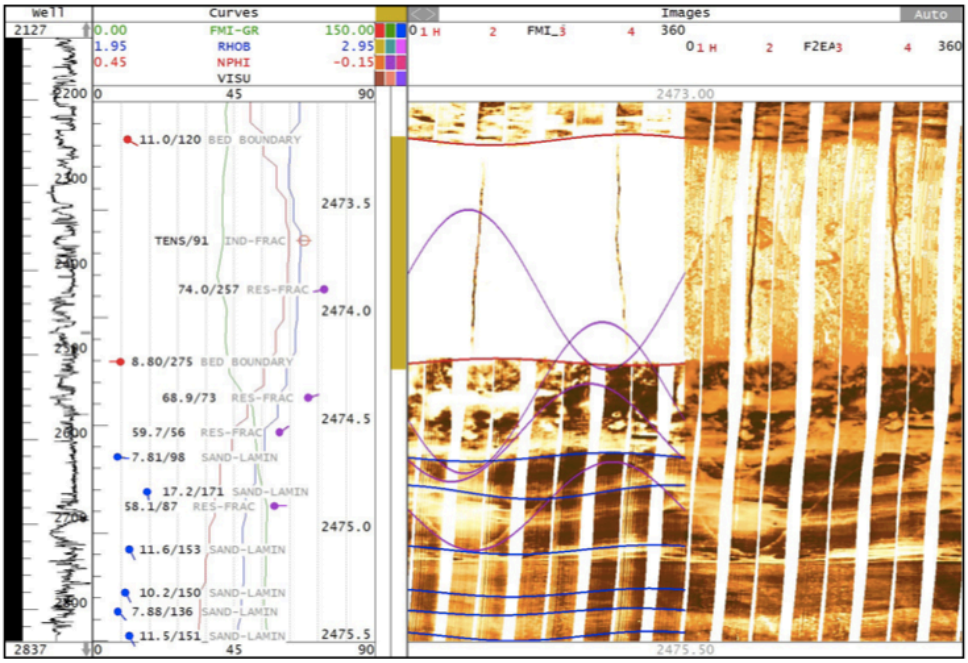


**Figure 26 Natural resistive fractures**

Conductive fractures are open natural fracture planes and are represented by the turquoise curve in the picture below (a resistive fracture is also seen in the top of picture):

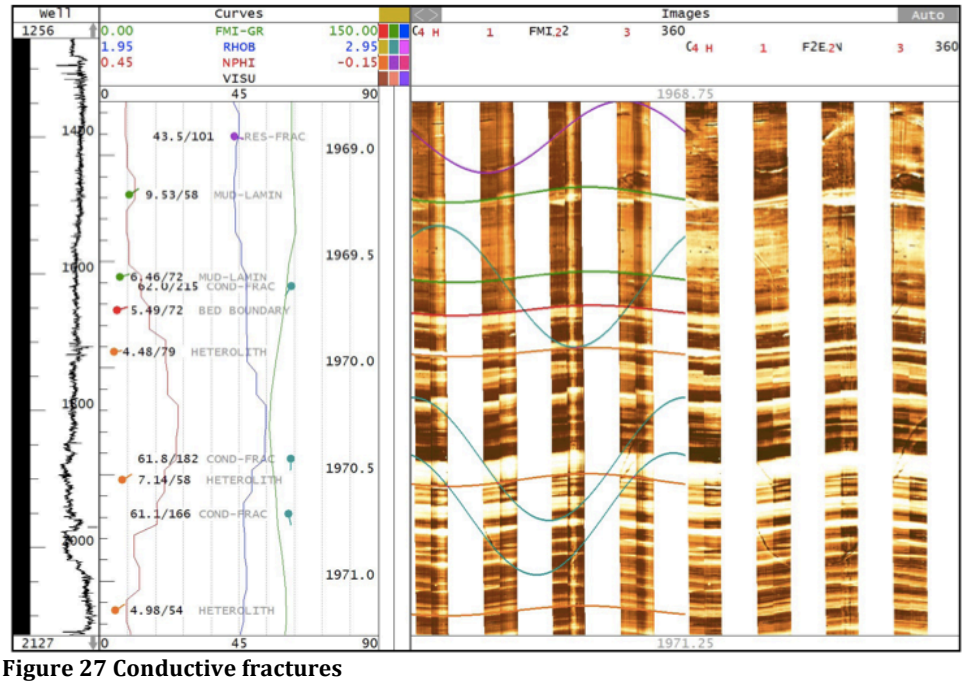


**Figure 27 Conductive fractures**

Finally, the drilling induced fractures demonstrates the known en echelon pattern, which then again display that the in-situ stress field is not aligned in the direction of the wellbore:

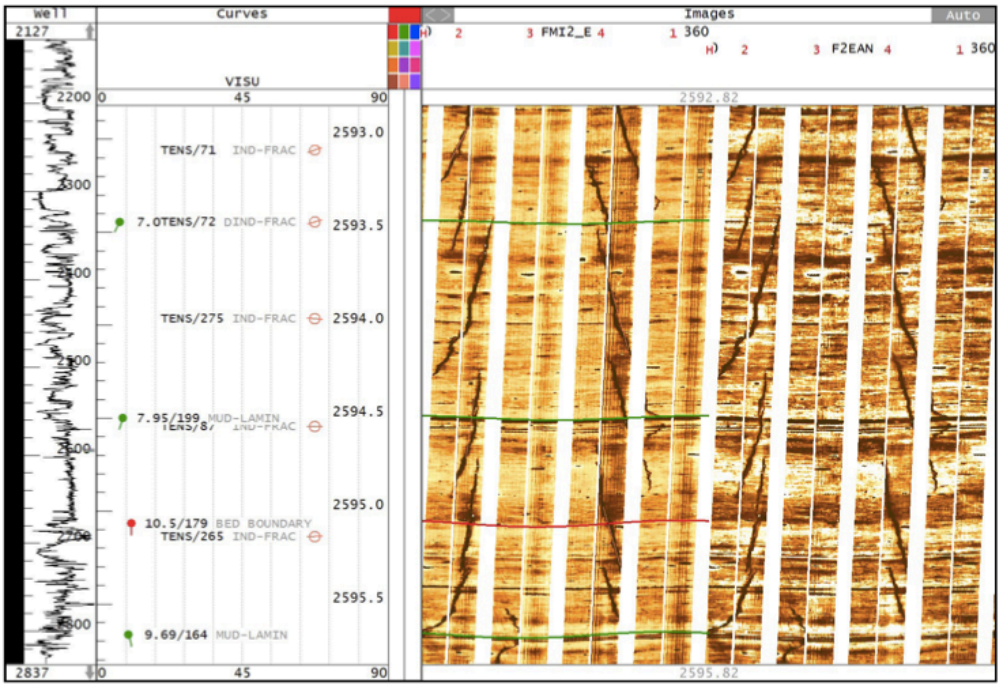


**Figure 28 Drilling induced fractures**

Another observation from the density log was that RHOB (bulk density) and NPHI (neutron porosity) always had high values. NPHI had an average of 33 % porosity, while RHOB had values around 2,65 g/cm$^3$. Gamma ray was also high, whereas this means that mudstone is present. This trend was seen in virtually all intervals were the drilling induced fractures occurred.

Drilling induced fractures were also seen on cemented borehole wall. The cemented intervals were defined as “weak zones” after major mud loss was encountered, hence cemented:

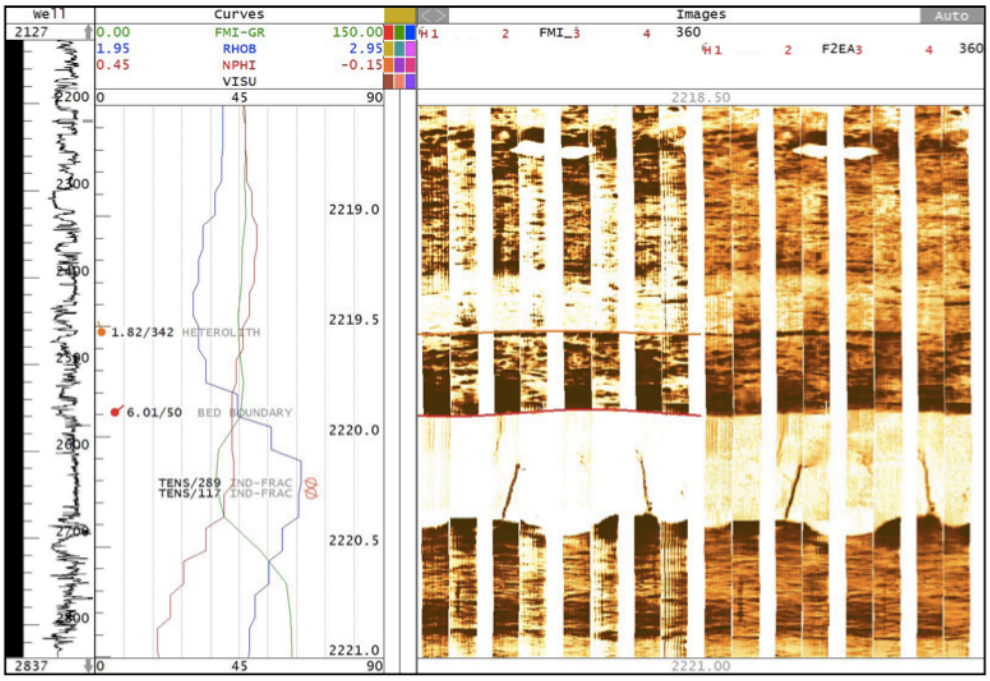


**Figure 29 Drilling induced fractures in cemented interval**

The majority of these zones were found in sandstone, whereas the drilling induced fractures that did occur in sandstone arose only in these intervals. The reason for that was suggested to be the relation of very high stress anisotropy in the stiff cemented sandstone (Eriksfiord, 2010).

### 9.3. Data analysis

The following table were obtained and will be used as the basis for the thesis' equations. The green columns represent data where drilling induced fractures were observed, while the colour beige represent data in the non-fracturing zones. The table also reveal that drilling induced fractures occur in mudstone formations, while absent in the formation that consisted of sandstone. Nevertheless, it is important to highlight that drilling induced fractures did not occur in *all* mudstone formations. Many of the fractures in the last section (six$^{th}$ and seven$^{th}$ column) were identified as *conductive induced fractures*, so the induced fractures developed from natural open joints. The formation's stratigraphi, lithology and depth are also listed.

**Table 7 Input data table**

| Input data | Drilling induced fractures | | | | | | | | | |
|---|---|---|---|---|---|---|---|---|---|---|
| | No fractures | | | | | | | | | |
| Stratigraphi | Kyrre Fm | Blodoeks Fm | Sognefjord 1 | Fensfjord 10 | Fensfjord 8 | Heather 1 | Rannoch Fm | | | |
| Lithology | Mudstone | Mudstone | Sandstone | Mudstone | Sandstone | Mudstone | Mudstone | | | |
| Depth [TVD] | 1852,8 | 1931,7 | 2166 | 2239,5 | 2292,5 | 2570,2 | 2726,5 | | | |
| | | | | | | | | | | |
| Poisson' ratio | 0,30 | 0,30 | 0,23 | 0,30 | 0,23 | 0,30 | 0,30 | | | |
| E [sg] | 1251,20 | 844,85 | 847,65 | 974,68 | 916,55 | 1258,03 | 1391,67 | | | |
| Sh [sg] | 1,21 | 1,23 | 1,27 | 1,23 | 1,27 | 1,22 | 1,22 | | | |
| SH [sg] | 1,44 | 1,43 | 1,44 | 1,48 | 1,45 | 1,59 | 1,53 | | | |
| Pore Pressure [sg] | 1,13 | 1,14 | 1,10 | 1,07 | 1,05 | 1,04 | 1,03 | | | |
| Mud Pressure [sg] | 1,21 | 1,23 | 1,23 | 1,23 | 1,22 | 1,22 | 1,22 | | | |
| α [°C^-1] | 0,000015 | | | | | | | | | |

E is the modulus of elasticity, and Sh & SH represents minimum and maximum horizontal stresses respectively. Unfortunately, the report does not state which models that are used in estimating these stresses. In that sense, these values have to be "dealt" with as they are, as error of uncertainty is not given accordingly. Also, the coefficient of linear thermal expansion, $\alpha$, is given as a constant for all litholgies as 0,000015 [°C^-1] since this value was not given.

All values were given in MPa and were converted to standard gradient, [sg], in accordance to mTVD, by the following equation:

$$P[bar] = 0{,}098 \cdot Z[m] \cdot d[sg]$$

**Eq. 29 Pressure**

Since 1 Bar = 10^5 Pa = 0,1 MPa, the gradient is derived by:

$$d[sg] = \frac{102 \cdot P[Mpa]}{Z[m]}$$

**Eq. 30 Standard gradient equation**

### 9.4. Assumptions

The following assumptions are stated for the equations applied in this study:

- First exploration well in the field, and none nearby wellbores
- Anisotropic stress state
- Vertical well
- Non-penetrating situation due to open hole section
- The elastoplastic barrier is neglected
- VFT is 81°C
- The coefficient of thermal expansion is assumed 0,000015/°C for all lithologies.
- The fracture gradient is analysed in the depth interval from 1852 - 2727 mTVD.

The calculated scaling factors based on the Poisson's ratio's for sandstone and mudstone are:

**Table 8 Scaling factors based on Poisson's Ratio**

| Lithology | Poisson's ratio | $K_{S1}$ | $K_{S2}$ |
|---|---|---|---|
| Sandstone | 0,23 | 0,617837 | 0,802 |
| Mudstone | 0,30 | 0,577073 | 0,824 |

These scaling factors were outlined in chapter 6.

## 9.5. Virgin Formation Temperature Gradient

The final well report claimed the VFT to be 4,12°C / 100 m. However, it also used MDT (Modular formation Dynamics Tester) logging tool in order to establish virgin formation temperature. These temperature recordings were taken approximately 14 hours after drilling the last section of the wellbore. The following table display the formation temperature trend found in the *Eriksfiord* (2010) report:

**Table 9 Temperature trend**

| Depth [mMD] | Temperature trend in formation |
|---|---|
| 300 - 1251 | 0,030 |
| 1251 - 2000 | 0,008 |
| 2000 - 2100 | 0,020 |
| 2100 - 2400 | 0,032 |
| 2400 - 2700 | 0,016 |

Due to poor quality in the image-log interval of 300 m from 2100 mMD, the temperature trend in the formation was assumed 3,25°C/100 m. Consecutively, the various reports interpreted distinct virgin formation temperatures, and the three trends that have been described are best presented by the following graph:

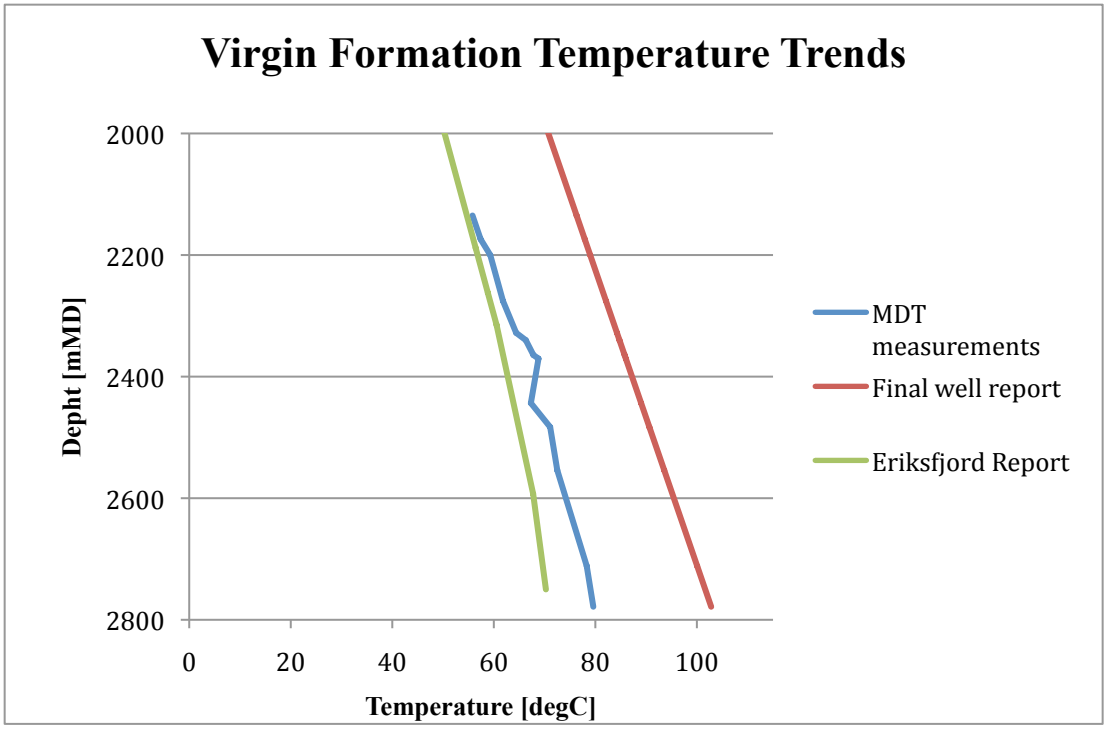


**Figure 30 Virgin Formation Temperature Trends**

As seen from the graph, the MDT measurements (blue line) are only logged in the interval from 2000 mMD to bottom of the well. Nevertheless, the gradients seem to have almost the same slopes, even though the curve by *Eriksfiord* (2010) (green line) construes the formation temperature to be much lower than the final well report (2006) does. Furthermore, details of when and how the temperature measurement where taken are not given. The thesis has chosen the MDT measurements (bottom hole temperature = 81°C) as its reference point for VFT, since the "Oil Directorate" also supported this BHT value (npd.no, 2012).

As seen from Figure 30, there are some irregularities around 2400 mMD. However, it is difficult to explain its cause since the temperature logging commenced after drilling (in order to conclude if drilling was the cause of the temperature change). However, a table that display the time of circulation during logging may explain the temperature change. The following table shows when circulation occurred, and the time between the circulations.

**Table 10 Bottom hole temperature**

| Run | Depth [mRBK] | Temperature [°C] | Time since circulation | Circulation time [min] |
|---|---|---|---|---|
| 1A | 2835 | 71 | 630 min | 90 |
| 1A | 2778,5 | 80 | 1430 min | 90 |
| 1A | 2834,6 | 71 | 1857 min | 90 |
| 1B | 2443,9 | 81 | 2212 min | 90 |

The fourth and last measurement was at 2444 mRBK, and the time since last circulation was the greatest of the four. This means that the well temperature had the greatest time in this run, to alter towards the VFT before circulation started. The measured bottom hole temperature was then 81°C, and the well was then circulated for 90 minutes. Nonetheless, it is important to underline that this argument is not a hard fact for the effective temperature change seen in the graph, as there can be several causes for this event.

### 9.6. Temperature behavior

It was with great disappointment that the thesis was not able to obtain a time-dependent temperature plot for the temperature inside the wellbore. This plot would make it possible to study and relate different situations that occurred during drilling towards the causes of temperature change, e.g. circulation. This time dependent temperature plot was (and is) of great importance for the thesis' study in order to achieve its primary purpose; if the thermal effect is the key cause of these drilling induced fractures. Consequently, three scenarios have been developed in order to give an interpretation of the thermal effect. Case one (red line), case two (green line) and case three (purple line) represents bottom hole temperature inside the wellbore at 70°C, 60°C and 40°C in the respective order.

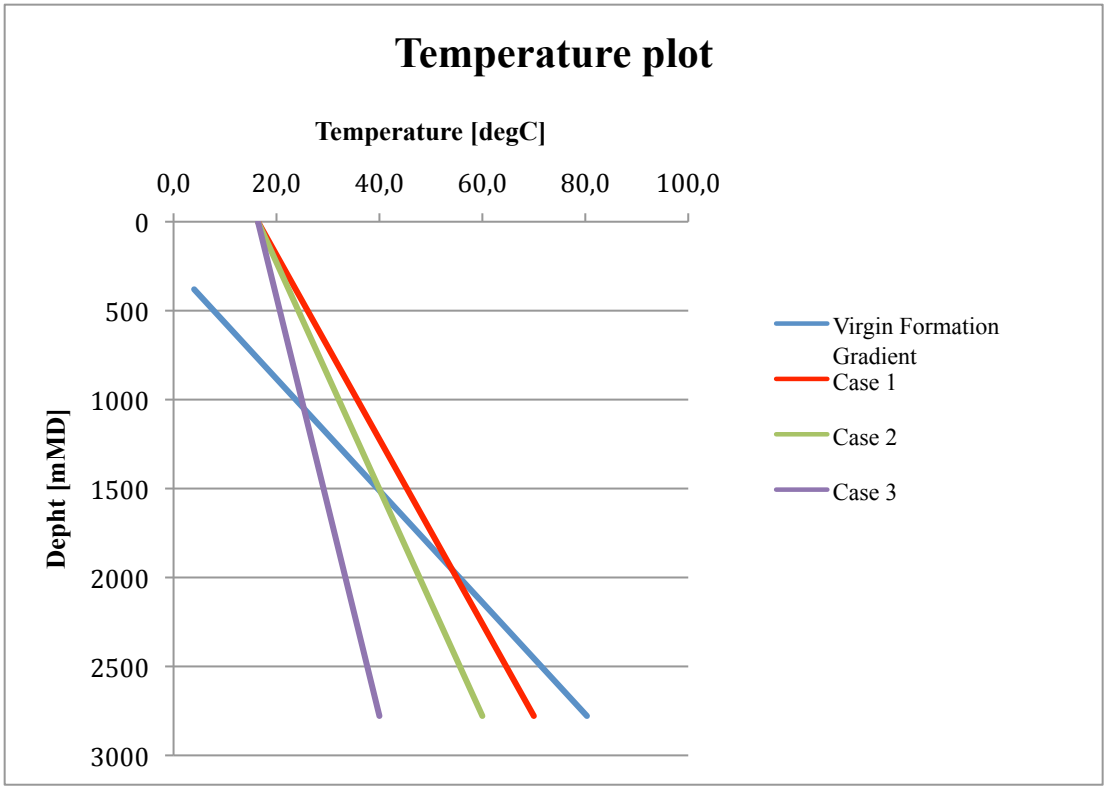


**Figure 31 Temperature Plot**

As seen from the plot, VFT gradient start from 380 mMD, which is the seafloor. The starting temperature is the average mud out temperature, which was 16,4°C. In reality, the wellbore temperature gradient will slightly decrease towards the bottom of the well (referring to Figure 21, page 40). The plot emphasize that as the inside temperature of the wellbore decreases, the delta towards the geothermal gradient increases. Thus, the fracturing gradient will shift towards left, and become more prone to failure. This will be demonstrated later in the chapter.

### 9.7. Estimating the fracturing gradient

The thesis has discussed several ways to predict the fracturing pressure. The following pressure plots highlights how diverse the fracture gradients are according to which model one chooses to use. Unfortunately, Matthews and Kelly method (which are often applied for offshore wells) are not included since the effective stress coefficient is absent.

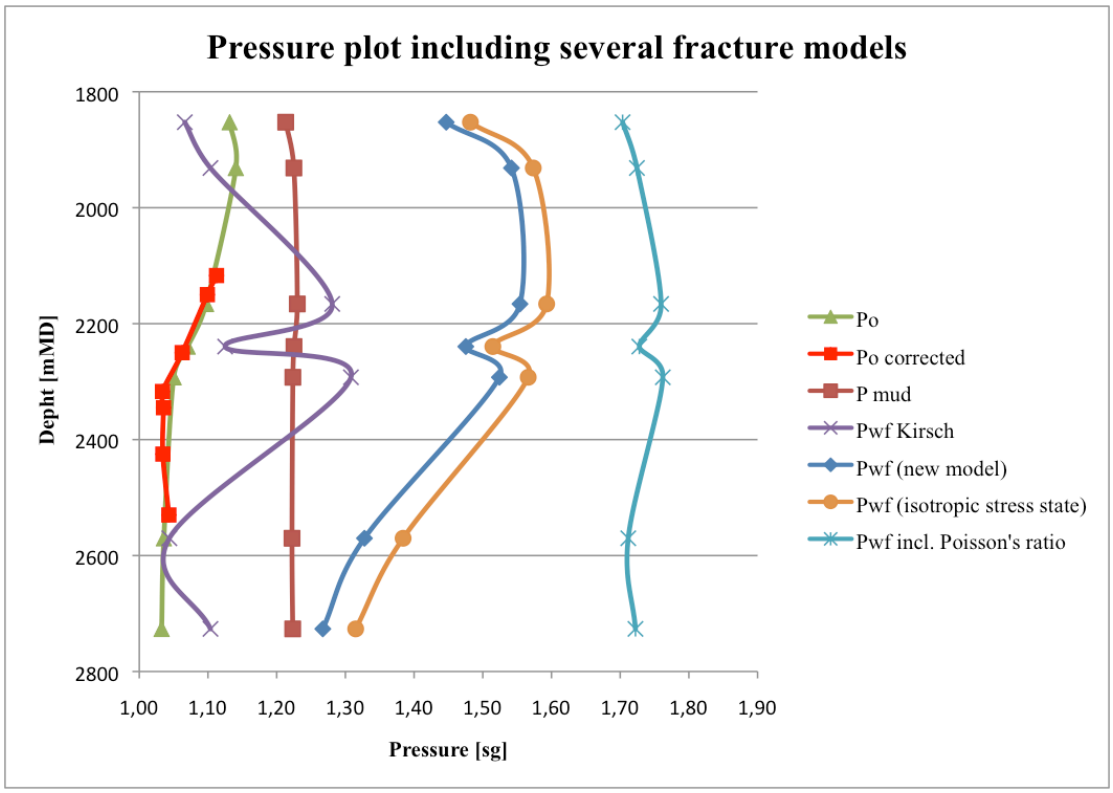


**Figure 32 Pressure plot**

Pore pressure and mud pressure data are obtained from Table 7, and the red line (Po corrected) is converted from a pressure plot obtained from the final well report to ensure its validity. These dots are also evident in Figure 25, which represents MDT measurements (real time measurements). The pore pressure curves correspond well.

As stated earlier in the thesis, Kirsch's equation (purple curve) demonstrates how strongly it underestimates the fracture gradient. On the contrary, the gradient that adds Poisson's ratio (turquoise curve) is less volatile, and seems to over-estimate the fracture gradient. This is also evident by the LOT test that was performed at 1259 mTVD, where it demonstrated that the formation should handle a pressure up to 1,46 sg. Moreover, it would be fair to question why this singular LOT is the reference point for maximum pressure throughout the whole wellbore, as the formation clearly changes its properties. That being questioned, it seems to be a procedure in today's drilling operations to perform several integrity tests at various depths in the formation.

Furthermore, the fracture gradient based on the new model is presented by the blue curve. The ΔT in the new model is the delta between the VFT of 81°C (which equals

a gradient of 3,18°C/100m) and the scenario for case 2, where BHT in wellbore is 60 °C. The thesis will discuss the three temperature scenarios in greater depth in the upcoming section. An isotropic stress state (orange curve) is also demonstrated in order to view how simplification can over-predict the fracture gradient. Moreover, temperature and Poisson's effect are included in the isotropic case, hence why the fracture gradient is close to the anisotropic stress state.

### 9.7.1. Fracture gradient with different wellbore temperatures

As previously discussed, temperature in the wellbore will vary during the drilling operation. The studied well was subjected to extensive mud loss according to the reports. Mud loss may decrease the effective wellbore temperature, and potentially cause drilling induced fractures. Three scenarios were previously stated, where case 1, 2 and 3 represent BHT in the wellbore at 70°C, 60°C, and 40°C respectively. The following plot demonstrates how the fracture gradient varies depending on different temperatures in the wellbore.

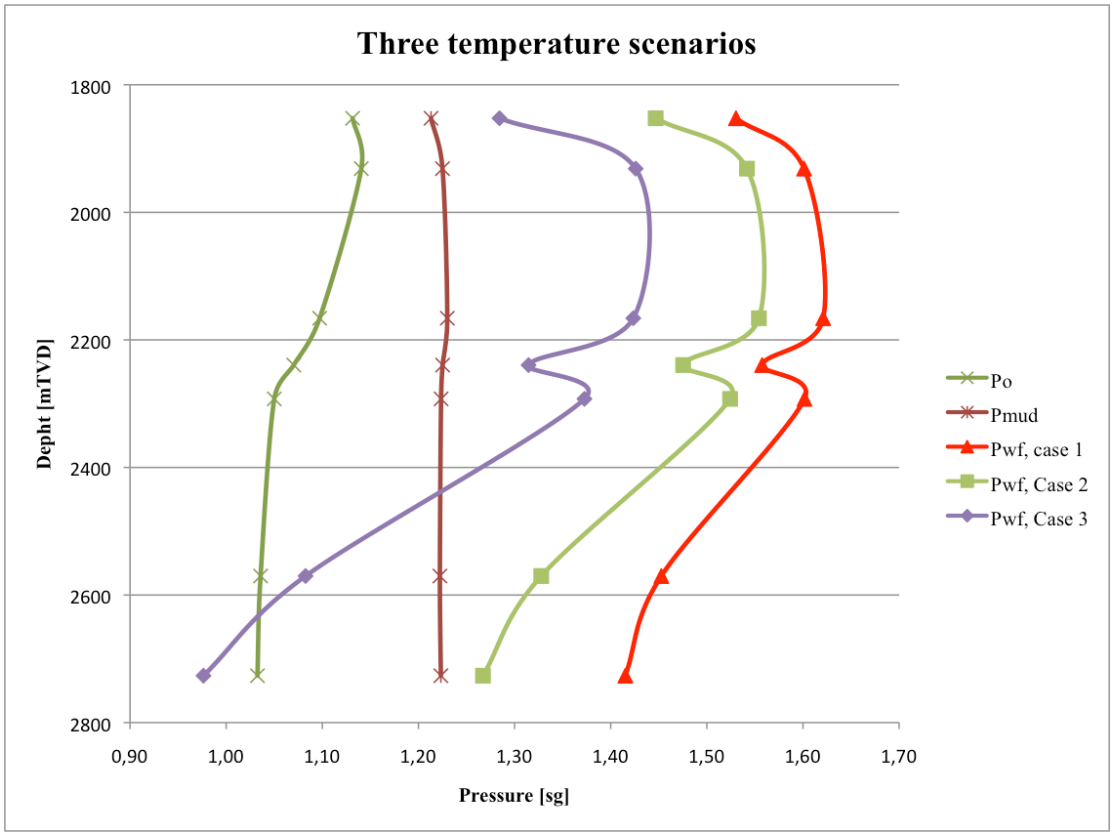


**Figure 33 Fracture gradient with three temperature scenarios**

The new fracturing model demonstrates that the fracture gradients are shifted towards right (wider mud-window) as temperature inside the wellbore increases, thus mud window increases. However, the gradients do not reveal a fracturing pattern that is consistent with the image log. This is because the real time-dependent temperature data could not be obtained, and therefore restricts the analysis' ability to investigate this further. Nevertheless, the curves describe their sensitivity towards changes in temperature. Additionally, all *points* that had proved drilling induced fractures had smaller pressure values than those without failure. The graph also display where swabbing was indicated.

### 9.8. Coefficient of thermal expansion

Another interesting observation was that the coefficient of thermal expansion seemed to have a greater impact on the fracturing gradient than initially presumed. This coefficient has often been ignored in the literature, and it has been difficult to find a "correct" value since those that have been measured (which were based on measurements from over 40 years ago), varies among the different sources (Huotari and Kukkonen, 2004). The following graph shows how the fracturing gradient for case 2 (BHT is 60°C) varies, when the coefficient of thermal expansion is taken into account for various formations. Moreover, since the coefficient of thermal expansion for mudstone was not found in the literature, *slate* replaced its value. The coefficient for slate is 9*10^-6/°C.

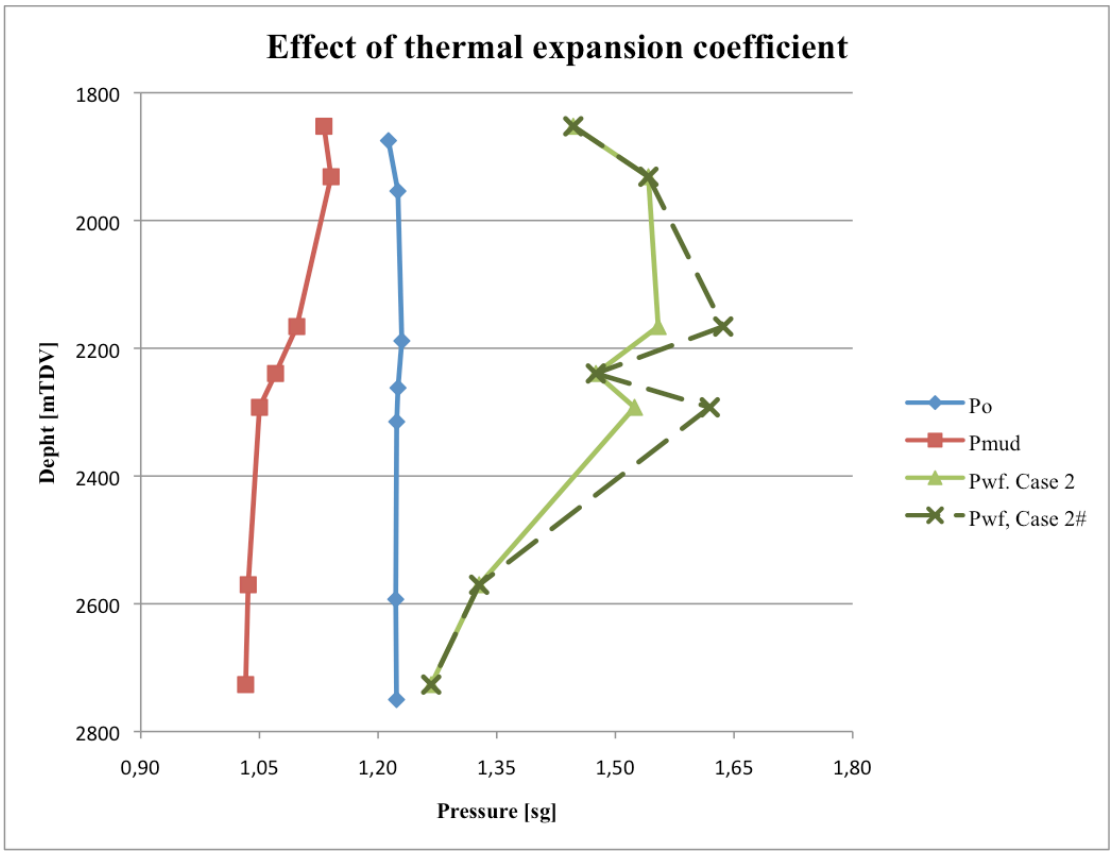


**Figure 34 Effect of thermal expansion coefficient**

The dashed green line represents the equation including the different coefficients for sandstone and slate, while the consistent green line only has the coefficient for sandstone. The coefficient seems to have a significant impact on the fracturing pressure curve as shown by the dashed line. Also, Huotari and Kukkonen (2004) stated that heating of rock may lead to fracturing of individual mineral grains, and further on to disaggregation of the rock since differences in thermal expansion results in stress concentrations at grain boundaries and contact points.

Furthermore, it is important to notice that some coefficients compiles low accuracy as they vary due to several influencing factors, e.g. relative proportions of different minerals, texture, initial porosity, constituent minerals, pressure and temperature. These are factors that make the coefficient of thermal expansion challenging to measure, as it also is anisotropic and dependent on different crystallographic orientation of minerals. Examples of its complexity have been proved through research, e.g. granite with big crystals was more sensitive to temperature than those

with small crystals (as cited in Amadei, 2001). Additionally, the number of heating and cooling cycles seems to increase thermal fracturing in the rock.

### 9.9. ECD measurements

A final important aspect to highlight is the measurement of ECD. The daily drilling report show variations in the mud density, though ECD was stable. The interesting aspect here is that it seems as ECD are based on surface data, and not by real-time dependent pressure data. The reported ECD has a straight vertical line, while one would expect it to change with depth due to increasingly hydraulic friction. One could therefore have a wrong interpretation of this pressure, as the calculated pressure would be lower than the *real* pressure and change in temperature has not been accounted for. The thesis has described how circulation can affect ESD, hence give a higher value of ECD.

## 10. Conclusion and further work

The thesis has analysed drilling induced fractures, where temperature effect has been weighted. A new fracturing model, which included Poisson's ratio, temperature effect, and an elastoplastic barrier, has also been investigated in this thesis. However, the latter was neglected due to lack of data. The following conclusions can be made:

- Temperature seems to have a significant effect on drilling induced fractures, as the three scenarios demonstrated that change in borehole wall temperature influences the effective fracture gradient. Furthermore, the borehole wall temperature can be influenced by many factors, thereby e.g. mud temperature, circulation, and swabbing. Several studies investigated throughout the thesis' analysis support that cooling generates a prone situation for fracturing, while heating seemed to increase the fracture gradient (less likely incidents of drilling induced fractures).
- The coefficient of thermal expansion seems to have a greater impact on the initiation of drilling induced fracturing, than initially presumed. Hence, the thesis encourages for further research on this coefficient in order to find the specific value of thermal coefficient for various rocks.

- Drilling induced fractures formed almost exclusively in the stiffer rock, consisting of mudstone. A suggested reason was the close relation of the tensile fracture generation to the rock mechanical properties.
- Effective ECD management could be an interesting aspect regarding drilling induced fractures. The thesis was not able to investigate if ECD could interpret these fractures due to lack of time-dependent downhole MWD data.

# 11. References


Aadnoy B S, 1990, *Inversion technique to determine the in-situ stress field from fracturing data,* Viewed 8 of March 2012 <www.onepetro.org>

Aadnoy B S, 2010, *Modern Well Design*, 2nd edition, Taylor and Francis Group, London, UK

Aadnoy B S and Belayneh M, 2009 *A new fracture model that includes load history, temperature, and Poisson's Effect* SPE Drilling and Completion

Aadnoy B S, Belayneh M, Arriado M, & Flatboe R, 2008 *Design of Well Barriers To Combat Circulation Losses"* Viewed 9 of March 2012 <www.onepetro.org>

Aadnoy B S and Bell J S, 1998 *Classification of Drilling Induced Fractures and Their Relationship to In-Situ Stress Direction,* Viewed 10 of February 2012 <www.onepetro.org>

Aadnoy B S and Chenevert M E, 1987 *Stability of Highly Inclined Boreholes,* Viewed 8 of March 2012 <www.onepetro.org>

Aadnoy B S, Cooper I, Miska S Z, Mitchel R F and Payne M L, 2009 *Advanced Drilling and well technology* p 443-544, Society of Petroleum Engineers

[2]Aadnoy B S, Hareland G, Kustamsi A, de Freitas T, and Hayes J, 2009 *Borehole Failure Related to Bedding Plane* Retriewed from dr. Eirik Kaarstad 27 April 2012, ARMA 09-106

Aadnoy B S & Looyeh R, 2011 *Petroleum Rock Mechanics: Drilling operations and Well Design*, Elsevier, Oxford, UK

Aadoy B S, Kaarstad E, and Belayneh M, 2007 *Elastoplastic Fracture Model Improves Predictions in Deviated Wells* Viewed 27 of February 2012 <www.onepetro.org>

Alberty M W & McLean M R, 2001 *Fracture Gradients in Depleted Reservoirs - Drilling Wells in Late Reservoir Life* Viewed 20 of March 2012 <www.onepetro.org>

Amadei B 2001 *Thermal and Hydraulic Properties of Rock,* Retrieved from Belayneh M. at the University of Stavanger April 2012.

Avasthi J M, Goodman H E, Jansson R P, 2000 *Acquisition, Calibration, and Use of the In Situ Stress Data for Oil and Gas Well Construction and Production* Viewed 20 of March 2012 <www.onepetro.org>

Asquith G, and Krygowski D, 2004, *Basic well log analysis*, AAPG Methods in Exploration 16, AAPG, Tulsa, Oklahoma

Chen G, & Ewy R T, 2005 *Thermoporoelastic Effect on Wellbore Stability,* Viewed 20 of March 2012 <www.onepetro.org>

Eriksfiord, 2010 *Geological interpretation from FMI, FMS and AND borehole Images,* Retrieved from Kaarstad E. at the University of Stavanger February 2012.

Final Well Report, 2006, Retrieved from Statoil **May** 2012.

Fjaer E, Holt R M, Horsrud P, Raaen A M & Risnes R, 2008 *Petroleum Related Rock Mechanics*, 2nd edition, Elsevier Amsterdam, The Netherlands.

glossary.oilfield.slb.com, Viewed 23 of February 2012
<http://glossary.oilfield.slb.com/search.cfm>
<http://www.glossary.oilfield.slb.com/Display.cfm?Term=swab>

Huotari T, and Kukkonen I, 2004 *Thermal Expansion Properties of Rocks: Literature Survey and Estimation of Thermal Expansion Coefficient for Olkiluoto Mica Gneiss*, Retrieved from Belayneh M, March 2012

Gonzales M E, Bloys J B, Lofton J E, Pepin G P, Schmidt J H, Nacuin C J, Ellis S T, and Laursen P E, 2004 *Increasing Effective Fracture Gradients by Managing Wellbore Temperature,* Viewed 7 of April 2012 <www.onepetro.org>

Hettema M H H, Bostrøm B, and Lund T, 2004 *Analysis of Lost Circulation During Drilling in Cooled Formations*, Viewed 23 of April 2012 <www.onepetro.org>

Islam M A, Skalle P, Al-Ajmi A M, and Søreide O K, 2010 *Stability Analysis in Shale through Deviated Boreholes using the Mohr and Mogi-Coulomb Failure Criteria*, Viewed 7 of March 2012 <www.onepetro.org>

Jaeger J C, Cook N G W, and Zimmerman R W, 2007 *Fundamentals of Rock Mechanics*, 4th edition, Blackwell Publishing

Kaarstad E, 1999 *Time-Dependent Temperature Behavior in Rock and Borehole.* PhD Thesis, University of Stavanger

Kaarstad E & Aadnoy B S, 1997 *Analysis of Temperature Measurements during Drilling,* Viewed 7 of April 2012 <www.onepetro.org>

Kaarstad E & Aadnoy B S, 1999 *Optimization of mud temperature and fluid models in offshore applications*, SPE 56939

Kaarstad E & Aadnoy B S, 2008 *Improved Prediction of Shallow Sediment Fracturing for Offshore Applications*, Viewed 27 of February 2012 <www.onepetro.org>

Khan S, Ansari S, Han H, and Khosavri N, 2012 *Understanding Shale Heterogeneity-Key to Minimizing Drilling Problems in Horn River Basin,* Viewed 27 of February 2012 <www.onepetro.org>

Kulander B R, Dean S L, Ward B J, 1990, *Fractured Core Analysis: Interpretation, Logging And Use of Natural And Induced Fractures in Core*, Viewed at AAPG Databases 15 of March 2012.

Li B, Al-Awadi M, Perrin C, Al-Khabbaz M, Al-Ashwak S, and Al-Qadeeri B, 2009 *Fracture and Sub-Seismic Fault Characterization for Tight Carbonates in Challenging Oil-Based Mud Environment – Case study From North Kuwait Jurassic Reservoirs*, Viewed 27 of March 2012 <www.onepetro.org>

Lorenz J C, Finley S J, & Warpinski N R, 1990 *Significance of coring-induced fractures in mesaverde core, Northwestern Colorado,* Viewed at AAPG Databases 15 of March 2012.

Ma T A, Lincecum V, Reinmiller R, and Mattner J, 1993 *Natura and induced fracture classification using image analysis*, Viewed 8 of February 2012 <www.onepetro.org>

MacPherson L A & Berry L N, 1972 *Prediction of Fracture Gradients from Log Derived Elastic Moduli*. Viewed 27 of February 2012 <http://www.onepetro.org>

Maury V & Guenot A, 1995 *Practical Advantages of Mud Cooling Systems for Drilling,* Viewed 27 of February 2012 <http://www.onepetro.org/mslib/app/Preview.do?paperNumber=00025732&societyCode=SPE>

Naturalfractures.com, Viewed 9 of March, 2012 <http://www.naturalfractures.com/1.3.5.htm>

Ndt-ed.org, Viewed 9 of March, 2012 <http://www.ndt-ed.org/EducationResources/CommunityCollege/Ultrasonics/EquipmentTrans/piezotransducers.htm>

Npd.no, Viewed 23 of March 2012 <http://www.npd.no/no/Rapportering/Bronner/>

OilGasGlossary.com, Viewed 23 of February 2012 <http://oilgasglossary.com/azimuth.html> , <http://oilgasglossary.com/swab.html>

Perkins T K & Gonzales J A, 1981 *Changes in Earth Stresses Around A Wellbore Caused by Radially Symmetrical Pressure and Temperature Gradient,* Viewed on 25 of April 2012 <www.onepetro.org>

Perkins T K & Gonzales J A, 1985 *The Effect of Thermoelastic Stresses on Injection Well Fracturing,* Viewed on 25 of April 2012 <www.onepetro.org>

Rabia H, 1985, *Oilwell Drilling Engineering. Principles & Practices*, Graham & Trotman UK

Rezmer-Cooper I, Bratton T & Krabbe H, 2000 *The Use of Resistivity-at-the-bit Images and Annular Pressure While Drilling in Preventing Drilling Problems*, Viewed on 5 of April 2012

<http://www.onepetro.org/mslib/app/Preview.do?paperNumber=00059225&societyCode=SPE>

Rezmer-Cooper I, Rambow F H K, Arasteh M, Hashem M, Swanson B, & Gzara K, 2000 *Real-Time Formation Integrity Test Using Downhole Data,* Viewed on 5 of April 2012 <www.onepetro.org>

Srivastav R, Enfis M, Crespo S, Ahmed R, Saasen A, Laget M, 2012 *Surge and Swab Pressures in Horizontal and Inclined Wells*, Viewed on 5 of April 2012 <www.onepetro.org>

Statoil, 2009,Viewed 29 of February 2012 <http://www.statoil.com/no/NewsAndMedia/News/2009/Pages/5JanGjoa.aspx>

Tingay M, Reinecker J & Muller B, 2008 *Borehole breakout and drilling-induced fracture analysis from image logs*, Viewed 24 of March 2012 <http://dc-app3-14.gfz-potsdam.de/pub/guidelines/WSM_analysis_guideline_breakout_image.pdf>

Van Steene M, Povstyanova M, Al-Attar H, Gheit D A E, Abutaleb M, Lantz J and Kareem S A, 2010 *Using Wellbore Stability Analysis to Improve Drilling Preformance – Case Study from The Western Desert, Egypt,* Viewed 15 of April 2012 <www.onepetro.org>

Zemanek J, Caldwell R L, Glenn E E, Holcomb S V, Norton L J, Straus A J D, 1969 *The Borehole Televiewer - A New Logging Concept for Fracture Location and Other Types of Borehole Inspection,* Viewed 15 of March 2012 <www.onepetro.org>

Zoback M L, Zoback M D, Adams J, Assumpcao M, Bell S, Bergman E A, ... Zhizin M, 1989 *Global patterns of tectonic stress*, p. 291-298, Viewed 5 of March 2012 <http://search.proquest.com/georef>